November 2021

ATP synthase: investigating its in vivo rotation and testing the inhibitory effects of diarylquinolines

Sarah Hassan Radwan
The American University in Cairo AUC

The American University in Cairo
School of Sciences and Engineering

ATP SYNTHASE: INVESTIGATING ITS *IN VIVO* ROTATION AND TESTING THE INHIBITORY EFFECTS OF DIARYLQUINOLINES

A Thesis Submitted to
The Biotechnology Graduate Program

in partial fulfillment of the requirements for
the degree of Master of Science in Biotechnology

By Sarah Hassan Radwan
Bachelor of Science in Chemistry

under the supervision of
Dr. Hassan M.E. Azzazy
Professor and Associate Dean for Graduate Studies and Research
and
Dr. Dirk Bald
Associate Professor

Fall 2011

The American University in Cairo

ATP SYNTHASE: INVESTIGATING ITS *IN VIVO* ROTATION AND TESTING THE INHIBITORY EFFECTS OF DIARYLQUINOLINES

A Thesis Submitted by
Sarah Hassan Radwan

To the Biotechnology Graduate Program
Fall 2011

In partial fulfillment of the requirements for
The degree of Master of Science in Biotechnology

Has been approved by

Thesis Committee Chair/Advisor: Dr. Hassan M.E. Azzazy
Professor and Associate Dean for Graduate Studies and Research, School of Sciences and Engineering, the American University in Cairo.

Thesis Committee Reader/Co-advisor: Dr. Dirk Bald
Associate Professor and Faculty Member of the Structural Biology Department, VU University Amsterdam, the Netherlands.

Thesis Committee Reader/Internal Examiner: Dr. Adham Ramadan
Associate Professor and Chair of the Chemistry Department, School of Sciences and Engineering, the American University in Cairo.

Thesis Committee Reader/External Examiner: Dr. Mohamed Gad
Professor of Biochemistry, the German University in Cairo.

Thesis Committee Observer: Dr. Amr Shaarawi
Professor and Dean for Graduate Studies & Research, School of Sciences and Engineering, the American University in Cairo.

_____	_____	_____	_____
Program Director	Date	Dean	Date

DEDICATION

This thesis is dedicated to my parents. Thank you for your support and love.

ACKNOWLEDGMENTS

I would like to thank my supervisor Dr. Hassan Azzazy for his continuous support throughout the three years of my study. I would also like to thank Dr. Dirk Bald for providing me with the opportunity to conduct my thesis project at the Structural Biology department at the VU University in Amsterdam, the Netherlands. I would like to thank all my colleagues at the laboratory in the Netherlands for making my stay a pleasant one. Last but not least, I would like to thank Bassem Shenouda and Mai Mansour for their continuous support and help.

ABSTRACT

The American University in Cairo

ATP SYNTHASE: INVESTIGATING ITS *IN VIVO* ROTATION AND TESTING THE INHIBITORY EFFECTS OF DIARYLQUINOLINES

By Sarah Hassan Radwan

Under the supervision of Dr. Hassan M.E. Azzazy and Dr. Dirk Bald

The rotation of the central subunits of ATP synthase relative to the surrounding parts has been observed by several techniques, however, most previous studies were carried out using the purified protein immobilized on glass slides or incorporated into liposomes. In this project, we labeled the enzyme using site-specific fluorescent tags, which would allow the observation of the enzyme's rotation *in vivo*. This system might also reveal if ATP synthase displays a favored resting position. To carry out these experiments, the a-subunit of the enzyme was fused to cyan fluorescent protein (CFP) while the γ-subunit was labeled with fluorescein arsenical hairpin binder (FlAsH), a small fluorescent probe. Fluorescence resonance energy transfer (FRET) experiments were carried out using inverted membrane vesicles and whole cells of *Escherichia coli*. Labeling with the site-specific fluorophores was successful and the labeled enzyme was functional. Moreover, FRET was observed between the two fluorescent labels in inverted membrane vesicles. The FRET efficiency was dependent on the nucleotides present, which may be due to a rotation-dependent FRET efficiency, but may also be explained by direct interaction between ATP and one of the used fluorophores. ATP synthase also represents a promising drug target for the diarylquinolines (DARQs) which can efficiently kill drug-sensitive and drug-resistant *Mycobacterium tuberculosis.* However, it is not known how DARQs interfere with the catalytic cycle of ATP synthase, a question which may be addressed using single-molecule detection techniques. *E. coli*, the most used bacterial model system, is resistant to DARQs at whole cell level. However, it is not known if this resistance stems from the lack of binding of DARQs to ATP synthase or from the possibility that ATP synthesis may not be essential for *E. coli* compared to *M. tuberculosis*. We tested if ATP synthesis in *E. coli* is susceptible to two different DARQs. Neither of the two DARQs showed high affinity for *E. coli* ATP synthase. However, one of them inhibited ATP synthesis at elevated concentrations (50% inhibitory concentration [IC_{50}] ~ 25 μM). These results will allow the use of single-molecule FRET experiments in *E. coli* to further investigate the mechanism of DARQ action.

TABLE OF CONTENTS

LIST OF TABLES

LIST OF FIGURES

LIST OF ABBREVIATIONS

9-AA: 9-aminoacridine

ACMA: 9-amino-6-chloro-2-methoxyacridine

ADP: adenosine diphosphate

AMP-PNP: adenylyl-imidodiphosphate

ATP: adenosine triphosphate

A.U. arbitary units

CCPGCC: cysteine-cysteine-proline-glycine-cysteine-cysteine

CFP: cyan fluorescent protein

DARQ: diarylquinoline

DCCD: NN'-dicyclohexylcarbodiimide

DMSO: dimethyl sulfoxide

EDTA: ethylenediaminetetraacetate

EGFP: enhannced green fluorescent protein

FlAsH-EDT_2: fluorescein arsenical hairpin binder-ethanedithiol

FRET: förster (fluorescence) resonance energy transfer

GFP: green fluorescent protein

GTP: guanosine triphosphate

HEPES: 4-(2-hydroxyethyl)-1-piperazineethanesulfonic acid

HIV: human immunodeficiency virus

IC_{50}: 50% inhibitory concentration

KDa: kilodalton

MDR: multi-drug resistant

MES: sodium 2-mercaptoethanesulfonate

MQ: milli Q

NADH: nicotinamide adenine dinucleotide

NADPH: nicotinamide adenine dinucleotide phosphate

Ni-NTA: nickel-nitrilotriacetic acid

$OD_{600\ nm}$: optical density at 600 nm

P_i: inorganic phosphate

RPM: revolutions per minute

SOC: super Optimal broth with Catabolite repression

TCEP: tris (2-carboxyethyl) phosphine hydrochloride

w/v: weight/volume

Wt: wild-type

XDR: extensively drug resistant

1. LITERATURE REVIEW

ATP synthase is one of the most important enzymes present in all living organisms (bacteria, chloroplasts, and mitochondria). It synthesizes ATP, the energy currency of living cells, from ADP and inorganic phosphate (P_i). It is a large protein complex (~500 kDa) consisting of two parts: a hydrophobic transmembrane portion, F_o, which is responsible for proton translocation across the membrane and a water-soluble portion, F_1, containing the catalytic nucleotide-binding sites and responsible for ATP synthesis/hydrolysis (Yoshida et al. 2001; von Ballmoos et al. 2009). ATP synthase uses a rotational mechanism to couple proton translocation with ATP synthesis making it the world's smallest motor (Boyer 1997). The enzyme synthesizes ATP using the energy of the proton motive force. This force drives the rotation of F_o which in turn causes the rotation of F_1 leading to conformational changes in the catalytic sites of F_1 necessary for ATP synthesis (Boyer 1997; von Ballmoos et al. 2009). The simplest form of the enzyme is the bacterial form, which has the following subunit composition: $\alpha_3\beta_3\gamma\delta\varepsilon$ for the F_1 portion and $a_1b_2c_{10\text{-}15}$ for the F_o portion (Figure 1). In *Escherichia coli*, the c-ring consists of 10 subunits whereas in other organisms it consists of 10 to 15 subunits (von Ballmoos et al. 2009). The enzyme could also be divided into a rotor (F_1 $\gamma\varepsilon$- F_o $c_{10\text{-}15}$) and a stator (F_1 $\alpha_3\beta_3\delta$- F_o ab_2) (Yoshida et al. 2001). The side stalk, which is made of the δ- and b_2-subunits, prevents the stator from being dragged by the rotor (Yoshida et al. 2001).

Several experiments were carried out to observe the rotation of the F_1 and F_o motors using different rotation markers. The rotation of the γ-subunit labeled with a fluorescent actin filament was observed during ATP hydrolysis using the F_1 part immobilized on nickel-nitrilotriacetic acid (Ni-NTA)-coated glass slides (Noji et al. 1997; Yasuda et al. 1998; Hisabori et al. 1999; Noji et al. 1999; Omote et al. 1999). It was shown that ATP hydrolysis drove a 360° unidirectional rotation of the actin filament in three 120° steps. The γ-subunit has also been labeled with smaller markers such as single fluorophores (Adachi et al. 2000) and 40-nm colloidal gold nanoparticles, which allowed the rapid rotation of F_1 and the resolution of the rotational substeps of the γ-subunit (Yasuda et al. 2001). It was found that the 120° rotational step consists of 90° and 30° substeps which were shown in later studies to be 80° and 40° substeps (Shimabukuro et al. 2003; Nishizaka et al. 2004; Adachi et al. 2007). Furthermore, manipulation of the rotation of the F_1 motor via redox switching or simultaneous optical and chemical stimuli has led to further understanding of how the enzyme can be regulated (Bald et al.

2001; Ristic et al. 2009). In these studies, the $\alpha_3\beta_3\gamma$ complex of F_1 was immobilized on a glass slide and the γ-subunit was labeled with single or duplex polystyrene beads and rotation was observed using a microscope. Single-molecule fluorescence resonance energy transfer (FRET) experiments have also been carried out to observe the stepwise rotation of the γ-subunit relative to the b-subunit using fully active F_oF_1-ATP synthase from *E. coli.* The individual double-labeled enzymes were incorporated into liposomes and rotation was observed during ATP synthesis and hydrolysis and was found to occur in opposite directions (Börsch et al. 2002; Diez et al. 2004).

The rotation of other subunits has also been observed during ATP hydrolysis such as the ε- and c-subunits which have been labeled with fluorescent actin filaments (Kato-Yamada et al. 1998; Sambongi et al. 1999; Pänke et al. 2000). However, rotation of the c-subunit was also observed for detergent-solubilized F_oF_1-ATP synthase with inactivated F_o. It was shown that detergents disrupt the F_oF_1 complex and F_1 could hydrolyze ATP regardless of the state of F_o. Therefore, the rotation of the c-subunit observed in this study and the previous ones could have been an artifact (Tsunoda et al. 2000). However, rotation of the c-subunit was later proved in a crosslinking study in which the γ-, ε- and c-subunits were crosslinked which did not affect ATP synthesis or hydrolysis (Tsunoda et al. 2001). Furthermore, the rotation of a single molecule of intact F_oF_1 was observed during ATP hydrolysis by attaching an 80-nm colloidal gold nanoparticle to the c-subunit of the immobilized F_oF_1. It was found that F_oF_1 performs ~350 revolutions per second at 37 °C and ~650 revolutions per second at 45 °C. The rotational behavior of F_oF_1 resembled that of F_1 which meant that F_o did not impose significant drag during ATP-driven rotation of F_oF_1 (Ueno et al. 2005). The stepwise rotation of the ε-subunit has been observed during ATP synthesis and hydrolysis with single-molecule FRET using F_oF_1 from *E. coli* and incorporated into liposomes revealing a joint rotation for the γε-complex (Zimmermann et al. 2005, 2006).

In all the previous studies, the enzyme was either immobilized on Ni-NTA-coated glass slides or incorporated into liposomes which are artificial environments. In addition, in previous FRET experiments, the FRET partners used were non-specific organic fluorophores, which did not allow their use *in vivo*. Only one group has observed the rotation of the a- and β-subunits relative to the c-subunit using membrane-embedded F_oF_1 (Tanabe et al. 2001; Nishio et al. 2002). The membrane fragments were immobilized on a glass slide through a His-tag connected to the

c-subunit. The results of their experiments suggested that the rotor and stator in ATP synthase are interchangeable depending on the immobilized subunit. Another group observed the rotation of the F_o motor with crosslinking studies using inverted membrane vesicles which also represent an *in vivo*-like environment (Suzuki et al. 2002).

Fluorescent labeling of proteins is usually carried out by reacting single cysteine residues of the target protein with thiol-reactive organic fluorophores (Hermanson 1996). Cysteine is very attractive since it is relatively rare in proteins and can be easily introduced into a protein by site-directed mutagenesis. Other reactive amino acids are too abundant in proteins and will not allow site-specific labeling of the target protein. The labeling is carried out *in vitro* after purifying the protein. To study labeled proteins inside living cells, the protein has to be purified, labeled, re-purified, and then reintroduced into the cell by either electroporation or microinjection, both of which are invasive techniques. Therefore, these studies are limited. The target protein cannot be labeled *in vivo*, since the fluorophores are non-specific and will bind to any available thiol groups in all proteins. To solve this problem, fluorescent proteins such as green fluorescent protein (GFP) have been used instead of organic fluorophores (Tsien 1998). These proteins are genetically fused to the target protein. Although this type of labeling is site-specific, however, fluorescent proteins are very large (~30 kDa) and can often be larger than the target protein itself disrupting the structure and function of the protein (Adams and Tsien 2008). These factors have led to the development of new protein labeling methods that are more specific and can be used *in vivo*. The tetracysteine-biarsenical system is an innovative technique, developed by Tsien and colleagues in 1998, for labeling proteins in live cells (Griffin et al. 1998). This system is based on the fact that arsenoixdes have a high affinity for closely-spaced cysteine pairs. Therefore, fluorescein arsenical hairpin binder-ethanedithiol (FlAsH-EDT_2) was designed which is a biarsenical fluorescein derivative and binds with high affinity to a motif made up of a rare six-amino acid sequence containing four cysteine residues (CCPGCC) (Griffin et al. 1998; Adams et al. 2002). This makes FlAsH highly specific and allows its use in labeling of proteins in intact cells. FlAsH is also membrane permeant and non-fluorescent by itself but becomes fluorescent only when bound to its motif (Griffin et al. 1998; Adams et al. 2002). Therefore, FlAsH-labeling causes minimal background fluorescence. Figure 2 shows the structure of FlAsH-EDT_2 (Invitrogen 2010). Furthermore, the FlAsH dye is small in size and therefore does not disrupt the structure or function of the enzyme. Figure 3 shows the difference in size between GFP and the

biarsenical-tetracysteine complex (Zhang et al. 2002). FlAsH emits green fluorescence (peak at ~528 nm) and is a good FRET acceptor from cyan fluorescent protein (CFP) (Figure 4) (Hoffman et al. 2005; Adams and Tsien 2008). In this project, the a-subunit of ATP synthase was fused to CFP while the γ-subunit was labeled with FlAsH and FRET experiments were carried out to observe the *in vivo* rotation of the enzyme.

In the phenomenon of FRET, there are two fluorophores, one acting as the donor and the other one as the acceptor (Didenko 2001). When the donor is excited, non-radiative excitation energy is transferred (through dipole-dipole interactions) from the donor to the acceptor which in turn gets excited and emits fluorescence. Thus, FRET causes the fluorescence intensity of the donor to decrease and that of the acceptor to increase. For FRET to occur, two conditions must be present. First, the emission spectrum of the donor must overlap with the absorption spectrum of the acceptor. This criterion is fulfilled with CFP and FlAsH. Secondly, the donor and acceptor should be within a certain distance known as the Förster radius (typically less than 10 nm). The Förster radius is defined as the distance between the donor and acceptor at which energy transfer efficiency is 50%. This criterion is also satisfied in ATP synthase since the diameter of the F_1 motor, which is the bulkiest part of the enzyme, is 10 nm (Lengeler et al. 1999). Therefore, two fluorophores in the same plane or close to each other will not exceed the 10 nm range allowing FRET to take place.

ATP synthase is an important enzyme since it also represents a potential drug target for the diarylquinolines (DARQs), a new class of anti-tuberculosis drugs. Tuberculosis is an airborne infectious disease that attacks the respiratory system and other organs resulting in an annual death of more than 1.7 million people (TB Alliance 2010). Almost one-third of the world's population is latently infected with *Mycobacterium tuberculosis* and every second someone is newly infected (WHO 2010a). HIV infection causes individuals to become more susceptible to tuberculosis infection or causes a latent infection to activate (Rosas-Taraco et al. 2006). In addition, co-infection speeds up the progress of both infections making tuberculosis a main cause of death among HIV-infected patients (Goletti et al. 1996; Mariani et al. 2001; TB Alliance 2010). The recommended standard treatment for tuberculosis requires the administration of four drugs: isoniazid, rifampicin, pyrazinamide and ethambutol or streptomycin for two months followed by isoniazid and rifampicin alone for four more months (WHO 2010b). For latent tuberculosis, the standard treatment is nine months of isoniazid alone (CDC 2000). The

mechanism of action of each drug is listed in table 1 (Rivers and Mancera 2008). However, these current anti-tuberculosis drugs are not very effective against dormant, non-replicating bacteria associated with latent tuberculosis. Furthermore, multi-drug resistant (MDR) and extensively drug resistant (XDR) strains have emerged (Rivers and Mancera 2008). MDR-tuberculosis is defined as tuberculosis which is resistant to at least isoniazid and rifampicin, the two most powerful first-line drugs. XDR-tuberculosis has resistance to isoniazid and rifampicin as well as second-line drugs and is almost incurable. Therefore, there is an urgent need for the development of new anti-tuberculosis drugs.

The DARQ lead compound, TMC207 (Figure 5), is able to inhibit both drug-sensitive and drug-resistant *M. tuberculosis in vitro* and *in vivo* (Andries et al. 2005) and can efficiently kill replicating as well as dormant mycobacteria. This makes DARQs potentially superior to the current anti-tuberculosis drugs (Koul et al. 2008; Rao et al. 2008). TMC207 was found to inhibit the bacteria by binding to subunit-c of ATP synthase (Koul et al. 2007). Furthermore, TMC207 is also highly selective towards mycobacterial ATP synthase with a 50% inhibitory concentration (IC_{50}) of 10 nM as opposed to an IC_{50} of >200 μM with human mitochondrial ATP synthase (Haagsma et al. 2009). Therefore, DARQs are unlikely to induce mitochondrial toxicity in mammalian cells and are promising drug candidates. However, it is not known how DARQs interfere with the catalytic cycle of ATP synthase. This information will be very useful for the design of novel ATP synthase inhibitor drug candidates. Insight in DARQ action may be obtained by single-molecule investigation of ATP synthase rotation. Since an experimental system for single-molecule analysis of mycobacterial ATP synthase is not available, therefore, in our experiments we used *E. coli* ATP synthase which is an established model system for single-molecule analysis. However, *E. coli* does not show susceptibility to DARQs at whole cell level (Andries et al. 2005), but it is not known if this resistance stems from lack of binding of DARQs to *E. coli* ATP synthase or from a lower importance of ATP synthase in *E. coli* metabolism compared to *M. tuberculosis*. In this project we tested if *E. coli* ATP synthase is susceptible to two different DARQ compounds.

2. INTRODUCTION

The importance of ATP synthase lies in the fact that it is the world's smallest biological motor and it is also a potential drug target for DARQs. For those two reasons, two sets of experiments were carried out. The aim of the first set of experiments was to label ATP synthase with site-specific fluorescent tags, which would allow the monitoring of the dynamics of ATP synthase using FRET measurements in an *in vivo* environment. Therefore, the a-subunit of ATP synthase was fused to CFP while the γ-subunit was incorporated with the tetracysteine FlAsH motif (CCPGCC) (Adams et al. 2002) to allow FlAsH to bind. If the enzyme was found functional after labeling, the ability of the introduced fluorophores for FRET would be determined. Subsequently, the nucleotide-dependency of FRET efficiency would be tested in inverted membrane vesicles and in whole *E. coli* cells to test suitability of this *in vivo* system as a potential marker for bacterial metabolism and to evaluate the possibility of a favored resting position for this enzyme.

The aim of the second set of experiments was to test the inhibitory effects of two selected DARQs (referred to as compound 1 and compound 2 in this report) on ATP synthesis in inverted membrane vesicles of *E. coli.* This would help in understanding why *E. coli* ATP synthase is resistant to DARQs at whole cell level. Furthermore, if inhibition of ATP synthesis occurred, this would allow the future use of *E. coli* ATP synthase as a model system in understanding the mechanism of inhibition of DARQs using single-molecule FRET analysis. For this experiment, we used the *E. coli* RA1 strain which is well suitable for single-molecule fluorescence analysis due to low background fluorescence. In addition, the a-subunit of ATP synthase was fused to enhanced green fluorescent protein (EGFP).

3. MATERIALS AND METHODS

Experiments for observation of *in vivo* rotation of ATP synthase:

3.1 Bacterial Strain I

ATP synthase was over-expressed in *E. coli* DK8 cells Δ(*uncB-C*), which lack the genes that code for the a- and ε-subunits of ATP synthase (Klionskv et al. 1984), using the PLZR10 expression plasmid. This plasmid codes for ATP synthase of the thermophilic *Bacillus* PS3, hence, stable at room temperature, with CFP fused to the C-terminus of the a-subunit of the enzyme and the tetracysteine FlAsH motif (CCPGCC) incorporated into the γ-subunit. As for the controls, PLZR9 plasmid was used to code for ATP synthase with CFP fused to the a-subunit. PLZR4 plasmid was used to code for ATP synthase with the FlAsH motif incorporated into the γ-subunit. PLZR10, PLZR9, and PLZR4 plasmids were all prepared by Dr. Zorica Ristic, VU University Amsterdam, the Netherlands. The plasmid pTR19-ASDS, prepared by Dr. Toshiharu Suzuki, Tokyo Institute of Technology, was used to code for ATP synthase lacking both CFP and the FlAsH motif. This control will be referred to as wild-type (wt) throughout the text.

3.2 Preparation of Electrocompetent Cells

A 5 mL LB [1% (w/v) tryptone (Oxoid, UK), 0.5% yeast extract (Oxoid), 1% NaCl (Sigma-Aldrich, Germany)] starter culture of *E. coli* DK8 cells was incubated overnight at 37°C with vigorous shaking. The following day, the culture was inoculated into 500 mL LB medium and the cells were incubated at 37°C at 180 rpm for ~5 hours until the $OD_{600\ nm}$ was 0.635. The cells were then spun down at 8000 rpm using a JA-10 rotor (Beckman Coulter, Germany) for 5 min at 4°C and the pellet was resuspended in 500 mL ice-cold 10% glycerol (Sigma-Aldrich). This step was repeated three times with resuspension in 250 mL ice-cold 10% glycerol followed by 85 mL and finally 1-2 mL. Aliquots of 50 µL were then prepared and snap-frozen in liquid nitrogen and stored at -80°C for later use.

3.3 Electroporation of Electrocompetent *E. Coli* DK8 Cells

Electrocompetent *E. coli* DK8 cells were transformed with the following four plasmids: PLZR4 (4Cysγ), PLZR9 (a_ECFP), PLZR10 (a_ECFP- 4Cysγ) and pTR19:ASDS (wt). 1-3 µL of each plasmid were transferred to an eppendorf tube containing 50 µL electrocompetent *E. coli* DK8 cells. The plasmid-cells mixture was then pipetted into an electroporation cuvette and placed in

the electroporator where the cells were zapped (voltage = 1.8 kilovolts). Around 300 µL of SOC solution was added to each mixture and transformed cells were incubated at 37°C for ~1 hour. The transformed cells were then plated onto LB plates [1% (w/v) tryptone , 0.5% yeast extract, 1% NaCl, 1.5% bacteriological agar (Sigma-Aldrich)] containing ampicillin (Sigma-Aldrich) and incubated overnight at 37°C.

The SOC solution was prepared by adding 97 mL water to 2 g tryptone, 0.55 g yeast extract, 1 mL 1 M NaCl, and 0.25 mL 1 M KCl (Sigma-Aldrich). This solution was then autoclaved and cooled to 55°C. Then, sterile solutions of 1 mL 1 M $MgCl_2$ (Sigma-Aldrich), 1 mL 1 M $MgSO_4$ (Sigma-Aldrich) and 1 mL 2 M glucose (Baker, the Netherlands) were added and the pH was adjusted to 7.0. The SOC solution was then divided into aliquots and stored at -20 °C.

3.4 Preparation of Inverted Membrane Vesicles

A 5 mL 2xYT [1.6% (w/v) tryptone, 1% yeast extract, 0.5% NaCl] starter culture containing ampicillin (final concentration = 100 µg/mL) was incubated for ~6-7 hours at 37°C and 220 rpm. The culture was then inoculated into 500 mL 2xYT medium containing ampicillin and incubated overnight at 37°C and 220 rpm. The following morning, the cells were spun down at 9000 rpm and 4°C for 15 min (rotor = JA-10). Cell pellets were resuspended with cold PA3 buffer [10 mM HEPES-KOH (Sigma-Aldrich), 5 mM $MgCl_2$, 10% glycerol, pH 7.5] containing the protease inhibitor, Pefabloc (Roche, Germany) using 7 mL buffer per 1 gram of cells. The cells were broken using the One Shot Cell Disrupter (Constant Systems, UK) after optimizing the conditions (single pass, pressure = 0.8 kbar). Cell debris and intact cells were spun down at 4000 rpm and 4°C for 20 min using a Beckman tabletop centrifuge. The supernatant containing the inverted membrane vesicles was then spun down at 55,000 rpm and 4°C for 1 hour using a Beckman ultracentrifuge and the 70 Ti rotor. Cell pellets were resuspended with cold PA3 buffer (1 mL) using a glass homogenizer. The sample was then divided into aliquots and snap-frozen using liquid nitrogen and stored at -80°C for later use. All previous steps were carried out in ice to ensure the stability of the vesicles.

Protein concentration of the four constructs was determined using the Bradford method (Bradford 1976). In this method, a solution of Coomassie brilliant blue G250 dye (Sigma-Aldrich) in dilute acid is added to the protein sample where it binds to the proteins and changes

color from brownish-orange (cationic form) to blue (anionic form). The absorbance of the mixture can then be measured at 595 nm and is directly proportional to the concentration of the bound dye and hence the concentration of proteins in the sample. Duplicate samples of serial dilutions (0, 10, 20, 30, and 40 µL) of a standard protein of known concentration [bovine serum albumin (Sigma-Aldrich), 1 mg/mL] were added to a fixed volume of the dye (500 µL) and MQ water in 1 mL total volume. Absorbance was measured at 595 nm and a standard curve of absorbance versus protein concentration was constructed. Protein samples of the four constructs were measured at 595 nm and their concentrations were determined using the standard curve.

3.5 CFP Fluorescence Detection

For each construct, in a 1.5 mL cuvette, 200 µL membrane vesicles was added to 400 µL buffer PA4 (10 mM HEPES-KOH, 100 mM KCl, 5 mM $MgCl_2$, pH 7.5). As a control, 10 µL CFP was added to 990 µL buffer PA4. The CFP plasmid was prepared by Dr. Zorica Ristic, VU University Amsterdam, the Netherlands. Fluorescence was measured for the five samples using a Varian Cary Eclipse fluorescence spectrophotometer (Germany) with the excitation wavelength set at 434 nm.

3.6 Proton Transport Assay

For each construct, in a 1.5 mL cuvette, 1.28 µL of 1 mM ACMA (Sigma-Aldrich) solution [dissolved in ethanol (Sigma-Aldrich)] was added to 1 mL buffer PA4 which was preheated in a water bath at 37°C. The cuvette was placed in the Varian Cary Eclipse fluorescence spectrophotometer where the excitation and emission wavelengths of ACMA were set at 410 and 480 nm, respectively and measurement was started. After ~2 min, 20 µL of membrane vesicles was added and when the baseline was constant, 15 µL of 200 mM ATP (AppliChem, Germany) solution (dissolved in MQ water and pH adjusted to 7.5 using NaOH) was then added. After ~ 12 min, 2.8 µL of 1 mM of an uncoupler solution, SF6847 (Sigma-Aldrich), which was dissolved in ethanol was added. Measurement was stopped after ~5 min.

3.7 Site-Specific Labeling and FRET Assay in Membrane Vesicles

After optimization of conditions and reagent concentrations, site-specific labeling was carried out as follows: to a 1.5 mL cuvette, 780 µL of buffer PA4, 20 µL of 50 mM TCEP (Pierce, USA)

solution, 100 µL of 50 mM MES (AppliChem) solution, 50 µL of membrane vesicles containing wt construct, and 50 µL of 100 µM FlAsH-EDT_2 solution (dissolved in buffer PA4) were added. TCEP and MES were dissolved in MQ water. The FlAsH dye was provided as a gift by Dr. Stephen Adams from the University of California, San Diego. The volumes of buffer PA4 and the vesicles were adjusted such that all four constructs had the same final protein concentration of ~1 mg/mL. Fluorescence was measured for each sample once after excitation at 434 nm and once at 508 nm at 0, 60 and 120 min. The cuvettes were covered with parafilm and stored in an incubator at 37°C between measurements to prevent evaporation of the samples.

3.8 Addition of Nucleotides to FlAsH-Labeled Membrane Vesicles

After two hours of FlAsH-labeling of the four constructs, 20 µL of buffer PA4 was added to each sample and fluorescence was measured at 434 nm and 508 nm. The same experiment was repeated four more times with the addition of 20 µL of 100 mM ADP (AppliChem) solution, 20 µL of 100 mM AMP-PNP (Sigma-Aldrich) solution, 20 µL of 100 mM ATP solution, and finally 20 µL of 100 mM GTP (AppliChem) solution. Fluorescence measurements were carried out at 434 nm and 508 nm. All the solutions of the nucleotides were dissolved in buffer PA4.

3.9 Preparation of Whole Cells

A 5 mL 2xYT starter culture containing ampicillin (final concentration = 100 µg/mL) was incubated for ~6-7 hours at 37°C and 220 rpm. The culture was then inoculated into 500 mL 2xYT medium containing ampicillin and incubated overnight at 37°C and 220 rpm. The following morning, the cells were spun down at 4000 rpm and 4°C for 20 min using the tabletop centrifuge. Cell pellets were resuspended with cold PA3 buffer containing Pefabloc using 7 mL buffer per 1 gram of cells.

3.10 Streaking Plates with FlAsH-Labeled Whole Cells

The following reagents were added to a cuvette: 140 µL buffer PA4, 10 µL of 50 mM TCEP solution, 50 µL of 50 mM MES solution, 250 µL of bacterial whole cells containing the PLZR10 plasmid (a_ECFP- 4Cysγ), and 50 µL of 100 µM FlAsH-EDT_2 solution. As a control, the same amounts of reagents were added to another cuvette but 50 µL of buffer was added instead of FlAsH-EDT_2. Both cuvettes were incubated at 37°C for ~3 hours. An LB plate containing

ampicillin was streaked with ~3 µL of one sample and another plate was streaked with ~3 µL of the other sample. Both plates were left overnight in an incubator at 37°C.

3.11 Site-Specific Labeling and FRET Assay in Whole Cells

After optimization of reagent concentrations, to a 1.5 mL cuvette, 480 µL buffer PA4, 20 µL of 50 mM TCEP solution, 100 µL of 50 mM MES solution, 300 µL of bacterial whole cells containing the PLZR9 plasmid (a_ECFP), and 100 µL of 100 µM FlAsH-EDT_2 solution were added. To another 1.5 mL cuvette, 280 µL buffer PA4, 20 µL of 50 mM TCEP solution, 100 µL of 50 mM MES solution, 500 µL of bacterial whole cells containing the PLZR10 plasmid (a_ECFP- 4Cysγ), and 100 µL of 100 µM FlAsH-EDT_2 solution were added. The volumes of buffer and whole cells were adjusted such that both constructs displayed the same fluorescence intensity of CFP and thus had approximately the same protein concentration. Fluorescence was measured for each sample once at 434 nm and once at 508 nm at 0, 60 and 120 min. The cuvettes were covered with parafilm and stored in incubator at 37°C between measurements. After two hours of FlAsH-labeling, 20 µL of 100 mM ATP solution (dissolved in buffer PA4) was added to both samples and fluorescence was remeasured at 434 nm and 508 nm.

3.12 Incubation with Glucose

The FRET assay was repeated once more where 280 µL buffer PA4, 20 µL of 50 mM TCEP solution, 100 µL of 50 mM MES solution, 500 µL of bacterial whole cells containing the PLZR10 plasmid (a_ECFP- 4Cysγ), and 100 µL of 100 µM FlAsH-EDT_2 solution were added to a 1.5 mL cuvette. The same volume of each reagent was added to another cuvette. Fluorescence was measured for both samples at 434 nm at 0, 60 and 120 min. After two hours of FlAsH-labeling, 25 µL of 1 M glucose solution was added to one sample to achieve a final concentration of 25 mM glucose. As a control, 25 µL of buffer PA4 was added to the other sample. Both samples were incubated in a water bath at 37°C with shaking at 300 rpm for 30 min and fluorescence was measured again at 434 nm. Samples were incubated once more at 37°C and fluorescence was remeasured at 70 min and 220 min.

Experiments for testing the inhibitory effects of diarylquinolines:

3.13 Bacterial Strain II

ATP synthase was over-expressed in *E. coli* RA1 cells (*unc*$^-$/cyo$^-$), which lack the F_oF_1 genes and genes coding for cytochrome c oxidase (Aggeler et al. 1997), using the pSD166 expression plasmid. This plasmid codes for the *E. coli* ATP synthase with EGFP fused to the C-terminus of the a-subunit of the enzyme. The *E. coli* RA1 cells transformed with the pSD166 plasmid were provided by Dr. Michael Borsch from Stuttgart University, Germany.

3.14 Preparation of Inverted Membrane Vesicles

Three different batches of inverted membrane vesicles of *E. coli* RA1 strain harboring the pSD166 plasmid were prepared using the same protocol described in section 3.4. Protein concentrations of the three batches were determined using the Bradford method described in section 3.4.

3.15 GFP Fluorescence Detection

In a 1.5 mL cuvette, 200 µL membrane vesicles of each batch was added to 400 µL buffer PA4 and fluorescence was measured using the Varian Cary Eclipse fluorescence spectrophotometer with the excitation wavelength set at 480 nm (specific for GFP).

3.16 ATP Synthesis Assay

The ATP synthesis assay was used to measure ATP synthesis and to test the inhibitory effects of compound 1 and compound 2 on *E. coli* ATP synthase. All samples contained inverted membrane vesicles of the *E. coli* RA1 strain with a protein concentration of 0.2 mg/mL, MOPS buffer [50 mM MOPS (AppliChem), 2 mM $MgCl_2$, pH 7.5], 11.8 U/mL hexokinase (Sigma-Aldrich), 100 µM diadenosine pentaphosphate (Sigma-Aldrich), 2 mM ADP, 25.4 mM glucose, and 20 mM KH_2PO_4 (Sigma-Aldrich). In total, there were 14 samples. Nine samples contained 5 µL of compound 1 dissolved in DMSO (Sigma-Aldrich) with different concentrations (0.1, 1, 5, 10, 17.5, 25, 50, 100 and 200 µM). As a control, 0.5 µL of 25 mM DCCD (Sigma-Aldrich) dissolved in ethanol was added to the tenth sample. To make sure that the solvents had no inhibitory effects on ATP synthesis, 5 µL of DMSO was added to sample 11 and 0.5 µL of 100% ethanol was added to sample 12. 10 µL of 250 mM NADH (AppliChem) was added to all

samples to start the reaction except one sample (sample 13) representing the background control (residual ATP). Sample 14 contained NADH without compound 1 and was used as the positive control representing maximum activity. All 14 samples were incubated in a water bath at 37°C and 300 rpm for 20 minutes. Reaction was stopped by adding 25 µL of 0.5 M EDTA (Sigma-Aldrich) to all the samples which were then transferred to ice. Samples were boiled for 5 min and centrifuged at 10,000 rpm for 20 min to get rid of denatured proteins. The synthesized glucose-6-phosphate is heat stable and does not denature upon boiling and remains in the supernatant. To start the ATP synthesis measurements, in a quartz cuvette, 2600 µL of MOPS buffer, 400 µL of the supernatant, and 30 µL of 250 mM $NADP^+$ (AppliChem) were added and mixed well. Using a Varian spectrophotometer with a wavelength set at 340 nm, $NADP^+$ was monitored for 1 min. To start the reaction, 5 µL of 1000 U/mL glucose-6-phosphate dehydrogenase (Sigma-Aldrich) was added and NADPH was produced. The same protocol was followed for compound 2 using also 5 µL of different concentrations (0.1, 1, 10, 25, 50, 100, and 200 µM).

4. RESULTS

Experiments for observation of *in vivo* rotation of ATP synthase:

4.1 Functionality of the CFP-ATP Synthase Fusion

In order to test the functionality of ATP synthase with site-specific fluorophores, inverted membrane vesicles were prepared from whole cells (Figure 6). The vesicles have their F_1 parts on the outside of their membranes and this is necessary to be able to carry out the proton transport assay described in section 3.6. The constructs were then tested for CFP fluorescence emission since CFP is fluorescent only when correctly folded (Reid and Flynn 1997; Craggs 2009). The constructs that had the CFP fusion (a_ECFP- 4Cysγ and a_ECFP) displayed the two maximum peaks characteristic of CFP at 475 nm and 502 nm. The other two constructs (4Cysγ and wt) that lacked CFP did not display the two peaks (Figure 7). This result indicates that CFP is correctly folded and functional in the fusion protein.

The next step was to ensure that ATP synthase in all four constructs was active and functional. Therefore, proton transport was monitored in each construct by fluorescence quenching of ACMA, a pH sensitive dye. Since the vesicles have their F_1 parts on the outside, they will be to hydrolyze the added ATP. Figure 8 shows the structure of ACMA which is a derivative of 9-AA. The vesicles were added to a solution of ACMA in buffer PA4. Reaction was initiated upon addition of ATP inducing ATP hydrolysis and causing protons to be pumped inside the vesicles which resulted in the quenching of ACMA. Upon addition of SF6847, an uncoupler, holes were formed in the membranes dissipating the pH gradient and restoring the fluorescence of ACMA. Figure 9 shows how proton transport is measured by fluorescence quenching of 9-AA (Taiz and Zeiger 2010). Figure 10 shows ACMA quenching between 75-80% for the four constructs which proves their activity. This experiment shows that ATP synthase is fully active in all four constructs before labeling with the second site-specific fluorophore.

4.2 Site-Specific Labeling and FRET in Membrane Vesicles

In order to introduce the second site-specific fluorophore, the four constructs were labeled with FlAsH-EDT_2 for two hours. The FRET signal was then measured at 0, 60, and 120 min once after excitation at 434 nm (specific for CFP) and once at 508 nm (specific for FlAsH). Figure 11 shows the fluorescence intensity of a_ECFP- 4Cysγ normalized to the wt (at 434 nm). After two

hours of FlAsH-labeling, the CFP peak (~475 nm) decreased and the FlAsH peak (~530 nm) appeared indicating successful FlAsH-labeling and FRET occurrence from CFP to FlAsH. The results of each construct alone at 434 nm are shown in Figure 12 and at 508 nm are shown in Figure 13. To ensure the activity of the membrane vesicles after two hours of FlAsH-labeling, proton transport measurements were carried out again. Figure 14 shows that the activity of the four constructs decreased after labeling, however, they were still active. These results show that ATP synthase after labeling with two site-specific fluorophores was still functional. Furthermore, energy transfer was successfully observed between the two fluorescent labels.

4.3 Nucleotide-Dependency of FRET Signal in Membrane Vesicles

Nucleotide-dependency of FRET efficiency is expected if ATP synthase displays one favorite resting state. Upon addition of ATP, the enzyme undergoes hydrolysis and its rotation should be detected by a change in the FRET signal before and after the addition of ATP. For this experiment, 2 mM nucleotides were separately added to each of the four constructs after two hours of FlAsH-labeling and changes in the FRET signal were observed. Figure 15 shows the results of this experiment using a_ECFP- 4Cysγ at 434 nm. The ratio of the fluorescence intensity of the donor to that of the acceptor (I_D/I_A) was calculated for each case with the donor peak chosen at 475 nm and the acceptor peak at 528 nm. The I_D/I_A before and after the addition of buffer PA4, 2 mM ADP, 2 mM AMP-PNP, and 2 mM GTP was almost the same. However, upon addition of 2 mM ATP, the I_D/I_A significantly changed from 0.81 to 1.10. Figure 16 shows the results of excitation at 508 nm where there is a significant decrease (around 60%) in the FlAsH peak (Figure 16-D) upon addition of ATP. The results of the control experiments (wt, 4Cysγ, and a_ECFP) at 434 nm and 508 nm are shown in Figures 17 through 22. These results show that the FRET signal changes upon addition of ATP which might be due to the rotation of the enzyme and hence the presence of a favorite resting position.

4.4 Nucleotide-Dependency of CFP Signal

In order to ensure that the effect of nucleotides on the FRET signal is due to the rotation of the enzyme and not an artifact, the effect of nucleotides on CFP alone was investigated. Fluorescence was measured before and after the separate addition of 2 mM ADP, 2 mM AMP-

PNP, 2 mM ATP, and 2 mM GTP to CFP (excitation wavelength = 434 nm). A greater decrease in the fluorescence intensity of the CFP signal was observed upon addition of ATP (Figure 23).

When 10 mM ATP and 10 mM ADP were separately added to CFP, a significant decrease in the CFP signal was observed with ATP. Figure 24 shows quenching of 25%, 34%, and 50% for buffer PA4, ADP and ATP, respectively. These results show that ATP has a quenching effect on the CFP signal and this means that the nucleotide-dependency of the FRET signal that was previously observed is not entirely due to the rotation of the enzyme.

4.5 Effect of FlAsH-EDT_2 on Whole Cells

The effect of FlAsH-EDT_2 on the survival of whole bacterial cells was tested since FlAsH contains arsenic which could be toxic to the cells. In order to do that, one plate was streaked with a solution of whole cells (harboring the construct a_ECFP- 4Cysγ) and 50 µL of FlAsH-EDT_2 and another plate was streaked with a solution containing 50 µL of buffer PA4 as a control. Figure 25 shows that there was no significant difference in the number of cells between the two plates which meant that FlAsH does not kill the bacterial cells.

FRET is difficult to observe in whole bacterial cells due to scattering as a result of the cytoplasmic constituents. However, we tried to test the FRET efficiency in whole cells using the two constructs, a_ECFP- 4Cysγ and a_ECFP. The FRET signal was measured at 0, 60, and 120 min once using an excitation wavelength of 434 nm and once at 508 nm. Figure 26 shows the FRET signal after two hours of FlAsH-labeling. The FlAsH peak (~530 nm) increases in a_ECFP- 4Cysγ, however, the CFP peak (~475 nm) decreases in both constructs. This result shows successful FlAsH-labeling in whole cells and the possibility of FRET occurrence from CFP to FlAsH.

Since ATP was found to have a quenching effect on the FRET signal in membrane vesicles, we sought to develop an ATP biosensor using whole cells. In order to do that, after two hours of FlAsH-labeling, 2 mM ATP was added to the two constructs (a_ECFP and a_ECFP-4Cysγ). The I_D/I_A before and after the addition of ATP was almost the same for the two constructs and there was no significant change in the FRET signal (Figure 27). These results suggest that the whole cells might be insensitive to the external addition of ATP since the catalytic sites are on the inside of the cells. Therefore, the cells were incubated with glucose to induce the production of ATP from within the cells. After two hours of FlAsH-labeling, 25 µL glucose (final concentration = 25 mM) was added to one sample containing bacterial cells

harboring the construct a_ECFP- 4Cysγ. As a control, 25 µL of buffer PA4 was added to another sample. Both samples were incubated at 37°C and the FRET signal was measured after 30, 70, and 220 min at 434 nm (Figure 28). Although the signal changes over time with a significant increase in the FlAsH peak, however, the graphs show no difference between the addition of glucose and the control experiment (addition of buffer PA4). This might be because the concentration of the glucose was too low.

Experiments for testing the inhibitory effects of diarylquinolines:

4.6 Inhibitory Effects of DARQs on ATP Synthesis in *E. Coli*

In order to test the inhibitory effects of DARQs on ATP synthesis in *E. coli*, three batches of inverted membrane vesicles of *E. coli* RA1 harboring the pSD166 plasmid were prepared, and GFP fluorescence was measured using an excitation wavelength of 480 nm. Figure 29 shows that the three batches contained the characteristic maximum peak of GFP which is at ~506 nm. This result indicates that GFP is correctly folded and functional in the fusion protein.

The ATP synthesis assay was then carried out to test the inhibitory effect of compound 1 on *E. coli* ATP synthase. Figure 30 shows the reactions of the ATP synthesis assay. Three independent experiments using the three different batches were carried out. Figure 31 shows the raw data of one of those experiments. After the addition of glucose-6-phosphate dehydrogenase, the sample lacking NADH showed little ATP synthesis since no NADPH was produced. The positive control showed maximum activity while DCCD, an inhibitor of oxidative phosphorylation, inhibited ATP synthesis, indicating functionality of this assay system. Figure 32 shows the mean values of the three experiments including standard deviation. At nanomolar concentrations, no significant inhibitory effect was visible. However, at elevated micromolar concentrations, compound 1 displayed dose-dependent inhibition of ATP synthesis with an IC_{50} of approximately 25 µM.

The ATP synthesis assay was also used to test the inhibitory effect of compound 2 on *E. coli* ATP synthase. Figure 33 shows the mean values of three independent experiments using standard deviation. Compound 2 did not show any inhibition of ATP synthesis when the experiments were carried out using MOPS buffer. When the experiments were repeated with buffer PA4, some inhibition occurred (Figure 34). The inhibitory effect, however, was lower compared to compound 1 with an $IC_{50} > 50$ µM and the dose-dependency was less pronounced.

5. DISCUSSION

Two sets of experiments were carried out in which the aim of the first set was to label ATP synthase using site-specific fluorescent tags. This would allow the observation of its *in vivo* rotation and to investigate the possibility of the presence of a favored position during the resting phase of the enzyme. The aim of the second set of experiments was to test the inhibitory effects of two DARQs on ATP synthesis in *E. coli.*

In the first set of experiments, the a-subunit of ATP synthase was fused to CFP while the γ-subunit was labeled with the FlAsH dye which is highly specific since it only binds to its tetracysteine motif (CCPGCC) which was incorporated into the γ-subunit. The high specificity of the FlAsH dye allowed its use *in vivo* which could not be carried out with other non-specific organic fluorophores. In addition, its small size did not disrupt the structure or function of the enzyme. The results showed that CFP was correctly folded and functional in the fusion protein and that ATP synthase was fully active in all four constructs after labeling with FlAsH as shown by the proton transport experiments in Figure 14. Therefore, site-specific labeling of ATP synthase in inverted membrane vesicles was successful. Furthermore, FRET was successfully observed from CFP to FlAsH (Figure 11).

The next step was to investigate the presence of a favored resting position for the enzyme. Mellwig and Bottcher (2003) established a three-dimensional map of ATP synthase from chloroplasts with a 20-Å resolution using electron cryomicroscopy data. This map provides a scaffold for fitting the known homology models of various subunits. It was suggested that in the inactive enzyme, the γ-subunit had a unique resting position relative to the side stalk in which the side stalk interacts with one specific α-subunit (Mellwig and Bottcher 2003). In this study, we tried to prove experimentally the presence of such a favored resting position in *E. coli* ATP synthase.

The rotation of the enzyme was observed by measuring the FRET signal before and after the addition of 2 mM nucleotides to the constructs. It was expected that in the case of buffer PA4, ADP and AMP-PNP, which is a nonhydrolyzable ATP analog, the FRET signal would be more or less the same since the enzyme is inactive in these three cases. In case of ATP, however, the enzyme undergoes hydrolysis and therefore should give a different signal before and after the addition of ATP. The buffer, ADP and AMP-PNP, as expected, did not cause any change in the FRET signal, while the addition of 2 mM ATP indeed caused a significant change in the signal.

However, Willemse et al. (2007) found that increasing levels of ATP decreased the fluorescence intensity of the acceptor in FRET experiments. According to the authors, ATP causes "a direct quenching of the energy-transfer step coupled to energy-induced charge displacement in the phosphate groups." If ATP was acting as a quenched acceptor, then ATP should have a direct effect on CFP. In order to test this hypothesis, 2 mM nucleotides were added to CFP, and it was found that ATP indeed showed a greater degree of quenching compared to the other nucleotides. This was even more evident when 10 mM ATP was added resulting in 50% quenching as opposed to only 25% and 34% for the buffer and ADP, respectively. The quenching that occurs, however, is not a result of resonance energy transfer from CFP to ATP since ATP has only one excitation peak at 260 nm (Dounce et al. 1948) which was verified by us and this absorption peak does not overlap with the emission spectrum of CFP. Furthermore, ATP seems to have a quenching effect on all four constructs including the ones that lack CFP as shown in Figures 17 through 20. It is known that ATP itself has fluorescent properties (Amat et al. 2005) and can quench the fluorescence of some chemical compounds (Li et al. 2005). Therefore, ATP might be able to quench the fluorescence of the FlAsH dye. This would explain the significant decrease (around 60%) in the FlAsH peak in the 4Cysγ construct which lacks CFP (Figure 20-D). Another possibility would be that ATP is able to bind to FlAsH through the oxygen atoms of its phosphate groups thus quenching its fluorescence. This could be possible since oxygen and sulfur have the same valence state. Furthermore, in a previous study, it was suggested that the hydroxyl group of the monothiol, 2-mercatoethanol could weakly bind to the arsenic atom of FlAsH (Adams and Tsien 2008). Figure 35 shows a possible structure of FlAsH with ATP binding to it.

In conclusion, it was difficult to determine whether the change in the FRET signal was due to the quenching effect of ATP or to the activity of the enzyme. In order to overcome this obstacle, GTP was used instead of ATP since both GTP and ATP support rotation of the enzyme (Noji et al. 2001). Addition of GTP to CFP did not show a significant decrease in the signal which meant that it did not have the same quenching effect of ATP. However, addition of GTP to the construct did not show any change in the FRET signal either. Therefore, the rotation of the enzyme and the presence of a favored resting position using inverted membrane vesicles were difficult to observe with ATP due to its quenching effect. Recently, a favored resting position for ATP synthases from chloroplasts has been observed using single-molecule FRET experiments

(Bienert et al. 2009). It was found that in the active state, the γ-subunit interacts with the three αβ-pairs with equal probability. In the inactive state, the γ-subunit interacts with only one specific αβ-pair which is in agreement with Mellwig and Bottcher's suggestion (Bienert et al. 2009).

The same experiments were repeated with whole bacterial cells where site-specific labeling was successful and FRET could be possible. However, a greater concentration of FlAsH was required to achieve a recognizable signal. We sought to develop an ATP biosensor using whole cells of *E. coli* by taking advantage of the quenching effect of ATP. First, 2 mM ATP was added to the whole cells after two hours of FlAsH-labeling, however, no change in the FRET signal occurred. This might have been because the F_1 parts, containing the catalytic sites, are on the inside of the bacterial cells making them insensitive to the external addition of ATP. This meant that the cells had to produce their own ATP from the inside for the FRET signal to change. In order to do that, the cells were incubated with glucose and the signal was measured after 30, 70, and 220 min (Figure 28). The FRET signal changed over time with a significant increase in the FlAsH peak, however, the same observations occurred with the control sample containing buffer instead of glucose. Furthermore, if ATP was responsible for this change in the FRET signal, then a decrease in the FlAsH peak should have been observed and not an increase. This increase in the FlAsH peak could be non-specific binding of the dye which could occur with time. The glucose concentration used in this experiment might have been too low and a higher concentration can be used to ensure the excess production of ATP in the cells allowing its detection before its complete consumption by the cells. Therefore, the development of the ATP biosensor needs further investigation.

In the second set of experiments, compound 1 displayed dose-dependent inhibition with an IC_{50} of ~25 μM. Compound 2 did not display any inhibition of ATP synthesis when the experiments were carried out using MOPS buffer. However, with buffer PA4, some inhibition occurred and this could be because buffer PA4 has a higher concentration of $MgCl_2$ (5 mM) than MOPS buffer (2 mM) and it is known that magnesium plays an important role in ATP synthesis (Ko et al. 1999). The inhibitory effect of compound 2, however, was lower (IC_{50} > 50 μM) than compound 1 and the dose-dependency was less noticeable. These results strongly indicate that the lack of DARQ-sensitivity observed for *E. coli* at whole cell level is at least in part explained by the low affinity of DARQs to *E. coli* ATP synthase. However, at higher concentrations,

inhibition of ATP synthesis was observed suggesting that *E. coli* ATP synthase may be used as a model system to investigate the mechanism of DARQs.

6. CONCLUSION AND FUTURE PLANS

In this project, there were two sets of experiments carried out highlighting the importance of ATP synthase not only as the world's smallest motor but also as a promising drug candidate. In the first set of experiments, site-specific labeling of ATP synthase in inverted membrane vesicles of *E. coli* with the FlAsH motif (CCPGCC) incorporated into the γ-subunit of the enzyme and CFP fused to the a-subunit has shown to be successful. In addition, FRET was successfully observed from CFP to FlAsH while maintaining the functionality of the constructs. This *in vivo*-like environment was the first step towards the *in vivo* observation of the enzyme's activity. However, the presence of a favored resting position for the enzyme was difficult to observe since it was difficult to distinguish between the quenching caused by ATP and the activity-dependant change in the FRET signal upon addition of ATP. This could be observed better using single-molecule FRET experiments. In addition, labeling with site-specific fluorophores in whole bacterial cells was successful and FRET observation might also be possible. The bacterial cells survived after around three hours of FlAsH-labeling. This *in vivo* labeling system could act as a marker for bacterial metabolism and may also form the basis for a potential genetically-encoded, FRET-based ATP biosensor. To further investigate this, an experiment will be carried out where a series of glucose concentrations will be used to find the optimum concentration which would result in the production of excess ATP thus allowing its detection prior to its complete consumption by the cells.

In the second set of experiments, it was shown that ATP synthase is a promising drug target of DARQs. Compound 1 has shown successful dose-dependent inhibition of ATP synthesis in inverted membrane vesicles of *E. coli* RA1 strain with an IC_{50} of approximately 25 μM. As for compound 2, some inhibition occurred but the inhibitory effect was lower compared to compound 1 with an IC_{50} of more than 50 μM and the dose-dependency was less obvious. The low affinity of DARQs to *E. coli* ATP synthase could be part of the explanation for the lack of DARQ-sensitivity observed for *E. coli* at whole cell level. However, the inhibition of ATP synthesis at higher concentrations suggests that *E. coli* ATP synthase may be used as a model system for future single-molecule experiments to investigate the inhibitory mechanism of DARQs.

7. TABLE

Table 1. Current first line anti-tuberculosis drugs and their mechanisms of action. (Table modified from: Rivers and Mancera 2008).

Drug	**Mechanism of action**
Isoniazid	Prodrug activated by *Mycobacterium tuberculosis* catalase-peroxidase. Inhibits mycolic synthesis in the cell wall of the bacteria.
Rifampicin (also known as Rifampin)	Inhibits transcription by interacting with the β-subunit of bacterial RNA polymerase enzyme.
Pyrazinamide	Prodrug converted by mycobacterial pyrazinamidases to active pyrazinoic acid. Lowers intracellular pH to a level that inactivates a vital fatty acid synthase.
Ethambutol	Inhibits arabinosyl transferase involved in cell wall biosynthesis.
Streptomycin	Inhibits protein synthesis by binding to the 30S ribosomal subunit preventing protein chain growth and recognition of mRNA triplet code.

8. FIGURES

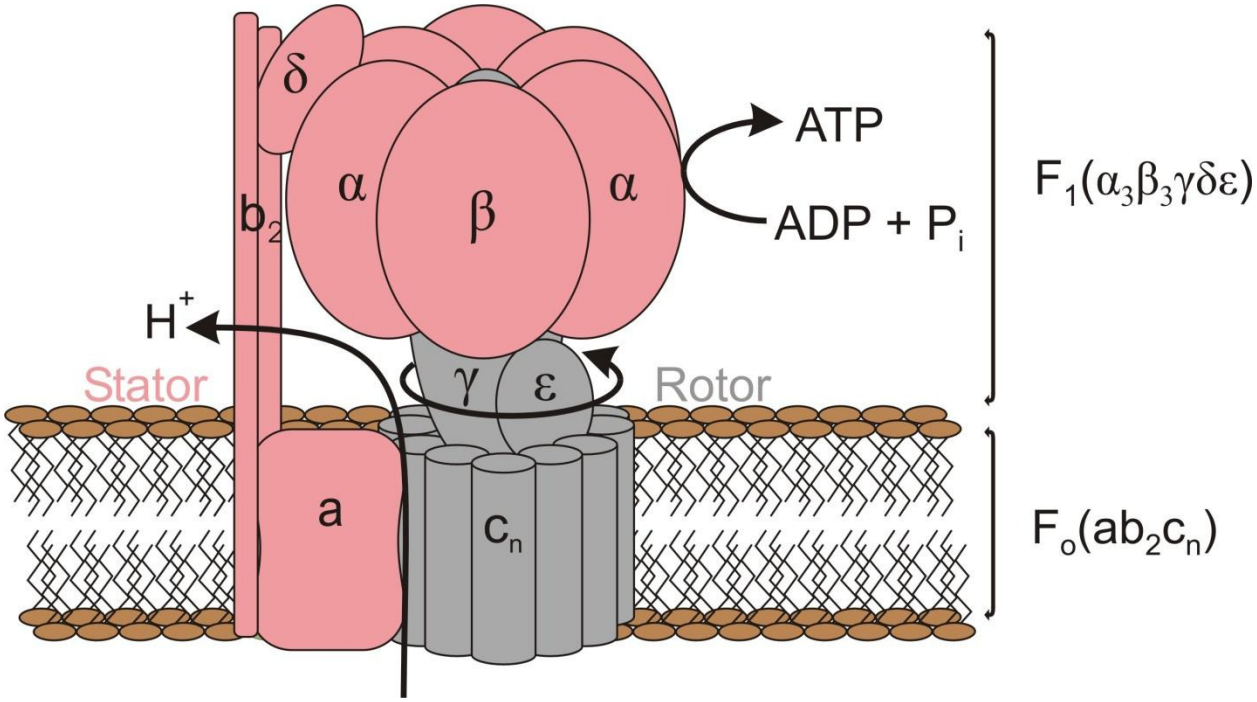

Figure 1. Structure of bacterial ATP synthase. The bacterial ATP synthase represents the simplest form of the enzyme. It consists of two protein complexes each acting as a motor: a transmembrane portion, F_o ($a_1b_2c_{10\text{-}15}$), and a water soluble portion, F_1 ($\alpha_3\beta_3\gamma\delta\varepsilon$). In *E. coli*, the c ring consists of 10 subunits whereas in other organisms it consists of 10 to 15 subunits. Mitochondrial ATP synthase has additional subunits in the F_o motor. In all organisms, the F_o motor is responsible for proton translocation across the membrane, whereas, F_1 is responsible for ATP synthesis/hydrolysis. The enzyme can also be divided into a rotor (F_1 $\gamma\varepsilon$-F_o $c_{10\text{-}15}$) and a stator (F_1 $\alpha_3\beta_3\delta$- F_o ab_2) in which the side stalk, consisting of the δ- and b_2-subunits, prevents the rotation of the stator with the rotor.

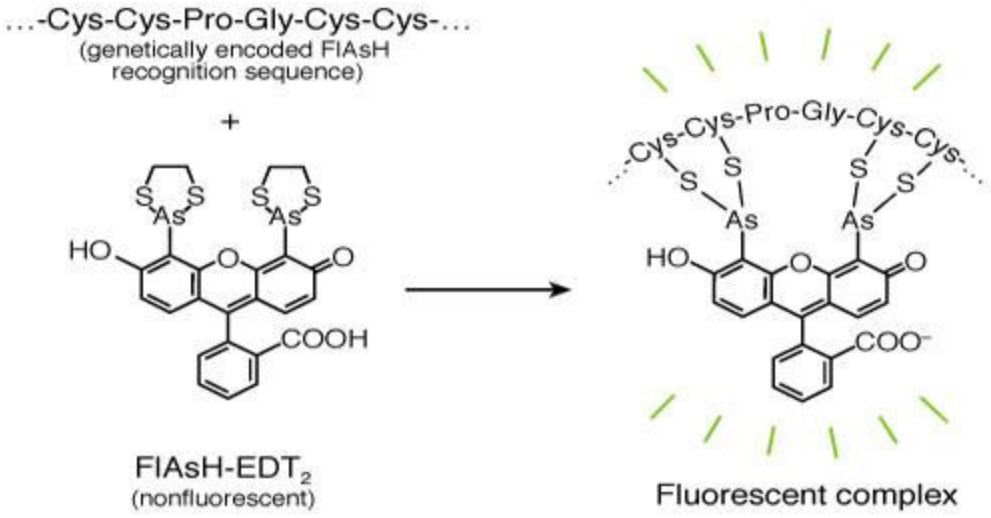

Figure 2. Structure of FlAsH-EDT$_2$. Fluorescein arsenical hairpin binder-ethanedithiol (FlAsH-EDT$_2$) is non-fluorescent by itself but in the presence of a tetracysteine motif (CCPGCC), the two molecules of EDT are replaced by the four thiol groups of the motif and the bound FlAsH becomes strongly fluorescent. The excitation and emission peaks of FlAsH-EDT$_2$ are 508 and 528 nm, respectively. (Figure reprinted from: Invitrogen 2010)

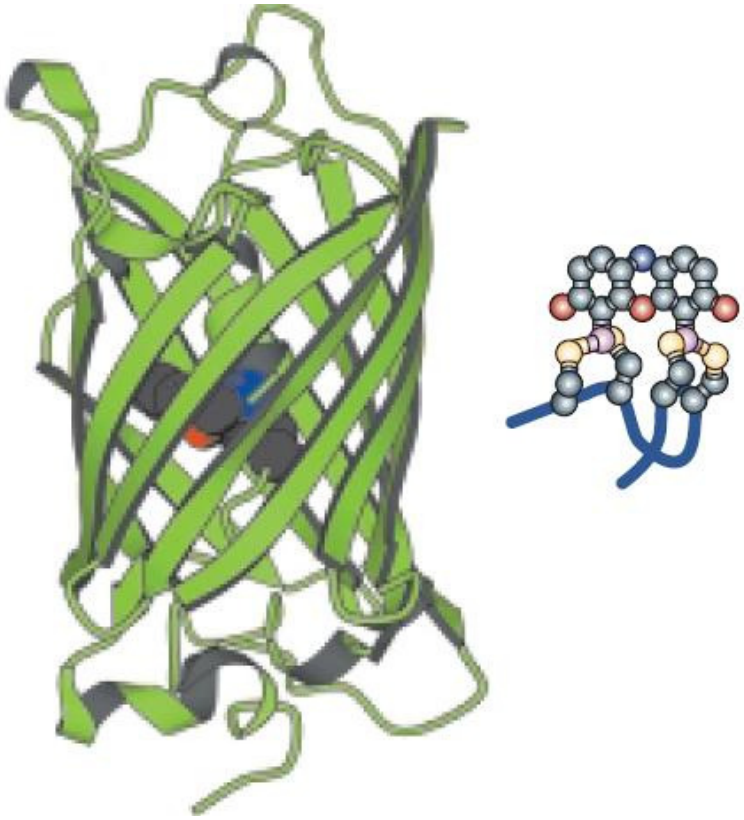

Figure 3. A comparison of the to-scale images of GFP and the tetracysteine-biarsenical complex. Green fluorescent protein (GFP) is composed of 238 amino acids and has a molecular weight of 27 kDa while the tetracysteine motif can be as short as 6 amino acids and the biarsenical-tetracysteine complex has a molecular weight of < 1 kDa. (Figure reprinted from: Zhang et al. 2002).

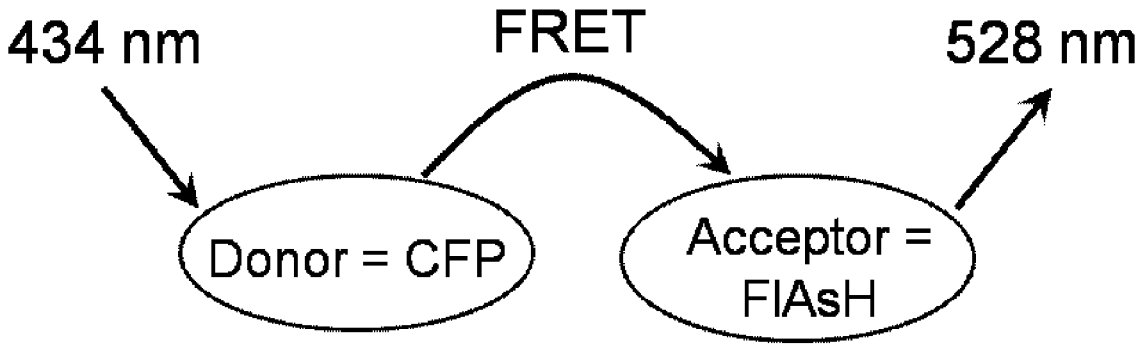

Figure 4. Schematic diagram showing FRET process from CFP to FlAsH. After labeling ATP synthase with the FlAsH dye, the cyan fluorescent protein (CFP) fused to the a-subunit is excited using a wavelength of 434 nm. Fluorescence resonance energy transfer (FRET) occurs from CFP to FlAsH which in turn gets excited emitting fluorescence with a peak at ~528 nm. For FRET to occur, the donor's emission spectrum must overlap with the acceptor's absorption spectrum. In addition, the donor and acceptor must be in close proximity (within 10 nm).

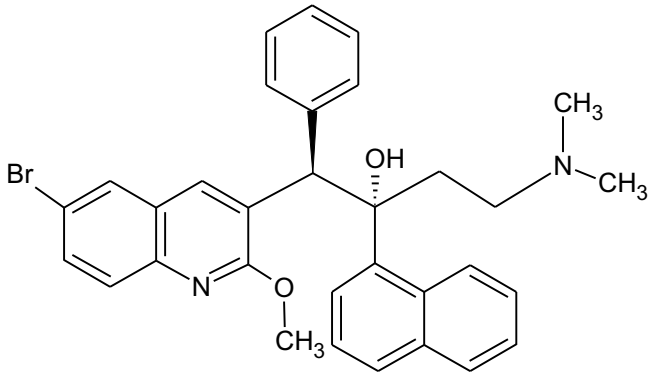

Figure 5. Structure of TMC207. TMC207 is the lead compound of diarylquinolines (DARQs), the new class of anti-tuberculosis drugs. TMC207 can inhibit both drug-sensitive and drug-resistant *M. tuberculosis in vitro* and *in vivo*.

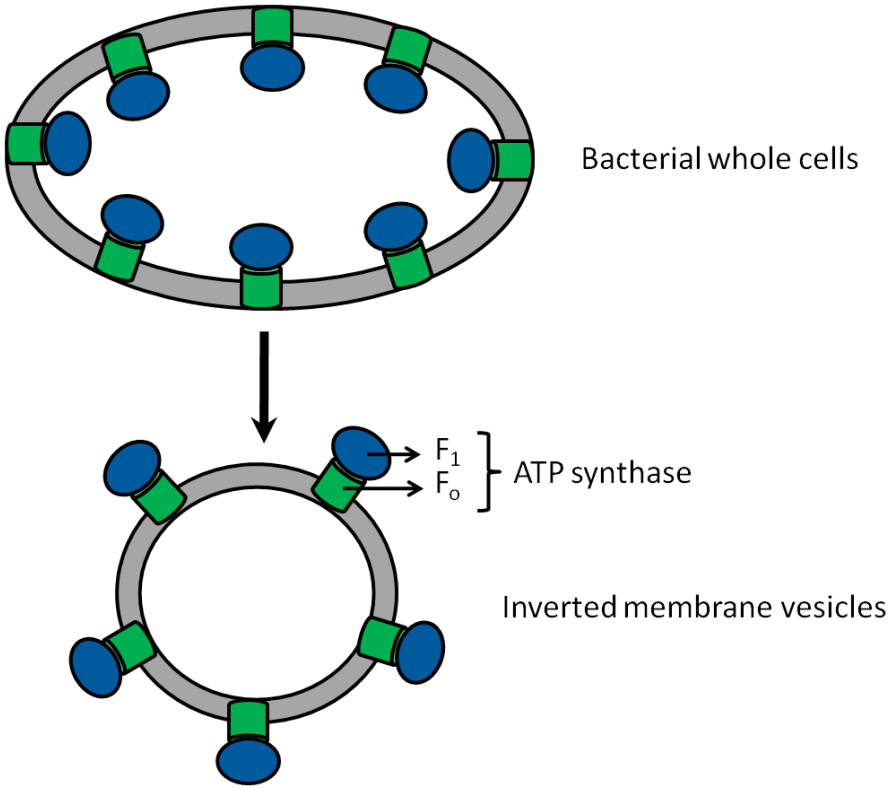

Figure 6. Schematic diagram showing the structure of inverted membrane vesicles. Bacterial whole cells are broken using the One Shot Cell Disrupter and cell debris and intact cells are spun down. The supernatant containing the inverted membrane vesicles is then spun down and cell pellets are resuspended with buffer. The inverted membrane vesicles produced from whole bacterial cells have the F_1 parts of ATP synthase on the outside of their membranes whereas the whole cells have their F_1 parts on the inside.

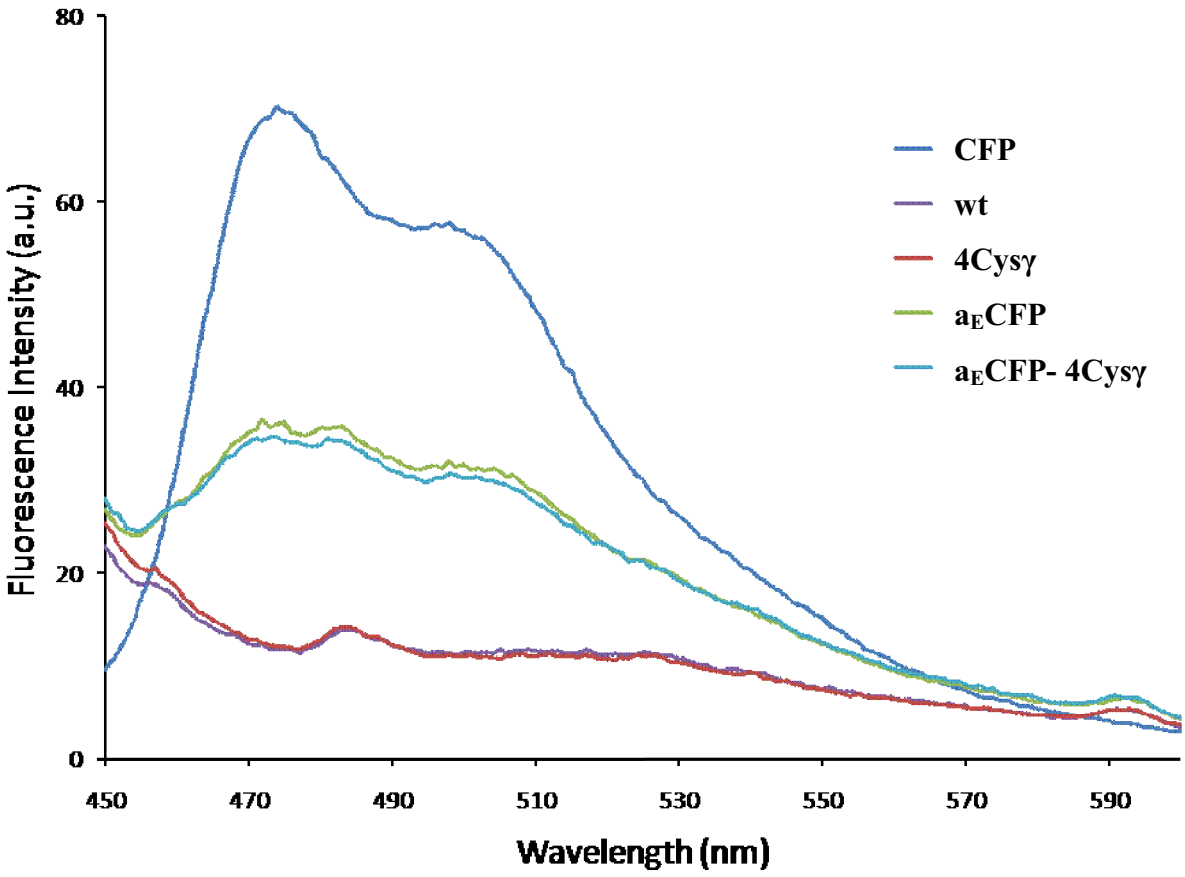

Figure 7. CFP fluorescence detection. The graph shows the fluorescence intensity of the four constructs (wt, 4Cysγ, a_ECFP and a_ECFP- 4Cysγ) and CFP as a control. Excitation wavelength was set at 434 nm. The two maximum peaks of CFP (~475 and ~502 nm) were present in both constructs containing CFP fused to the C-terminus of the a-subunit of ATP synthase (a_ECFP-4Cysγ and a_ECFP).

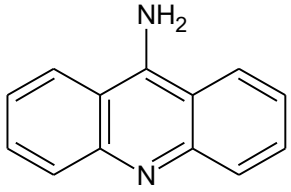

9-aminoacridine (9-AA)

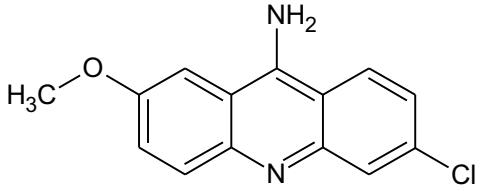

9-amino-6-chloro-2-methoxyacridine (ACMA)

Figure 8. Structure of ACMA and 9-AA. ACMA is a derivative of 9-AA. Both dyes are pH sensitive and can be used in monitoring proton transport in membrane vesicles.

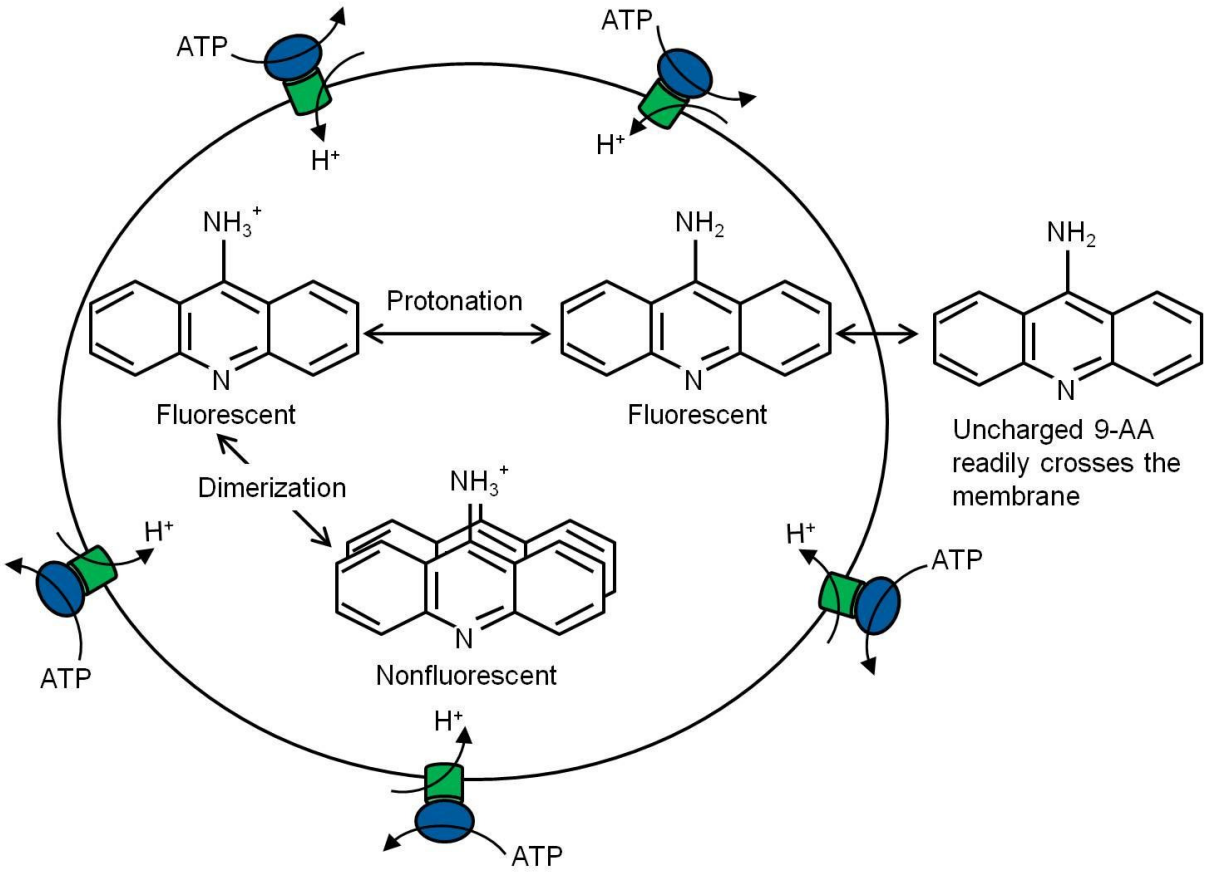

Figure 9. Proton transport measurement by fluorescence quenching. Uncharged fluorescent 9-aminoacridine (9-AA) readily crosses the membrane. Upon addition of ATP, ATP hydrolysis takes place causing protons to be pumped inside the vesicles. 9-AA becomes protonated and eventually forms dimers which results in the quenching of 9-AA. Upon addition of an uncoupler, holes are formed in the membranes dissipating the pH gradient and restoring the fluorescence of 9-AA. (Figure modified from: Taiz and Zeiger 2010).

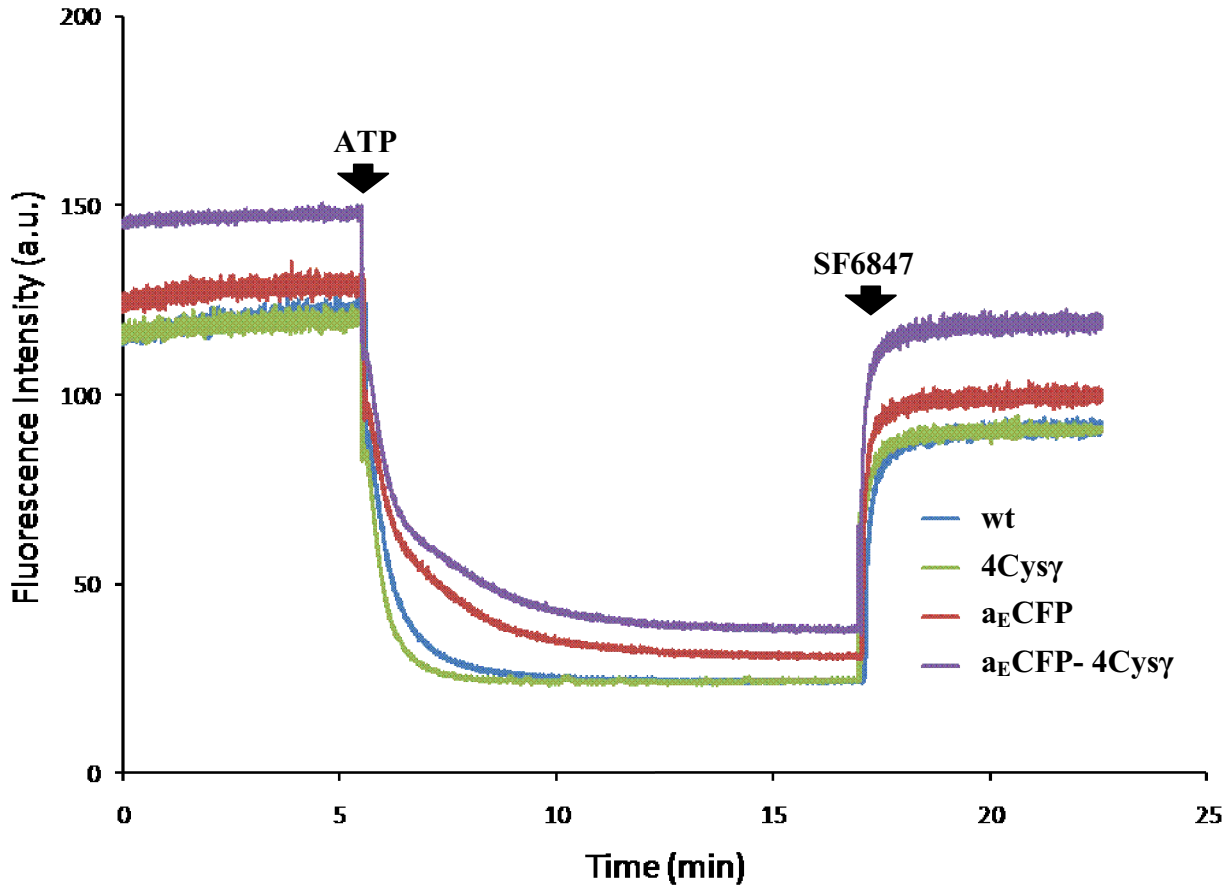

Figure 10. Proton transport measurement of inverted membrane vesicles before FlAsH-labeling. To confirm the functionality of ATP synthase in all four constructs (wt, 4Cysγ, a_ECFP and a_ECFP- 4Cysγ), proton transport was monitored by fluorescence quenching of a pH sensitive dye, ACMA. The membrane vesicles were added to a solution of ACMA in buffer in a cuvette which was placed in a Varian Cary Eclipse fluorescence spectrophotometer. The excitation and emission wavelengths were set at 410 and 480 nm, respectively. Reaction was initiated upon addition of ATP inducing ATP hydrolysis and causing protons to be pumped inside the vesicles hence quenching the fluorescence of ACMA. Upon addition of SF6847, the uncoupler, holes were formed in the membranes causing protons to escape and restoring the fluorescence of ACMA.

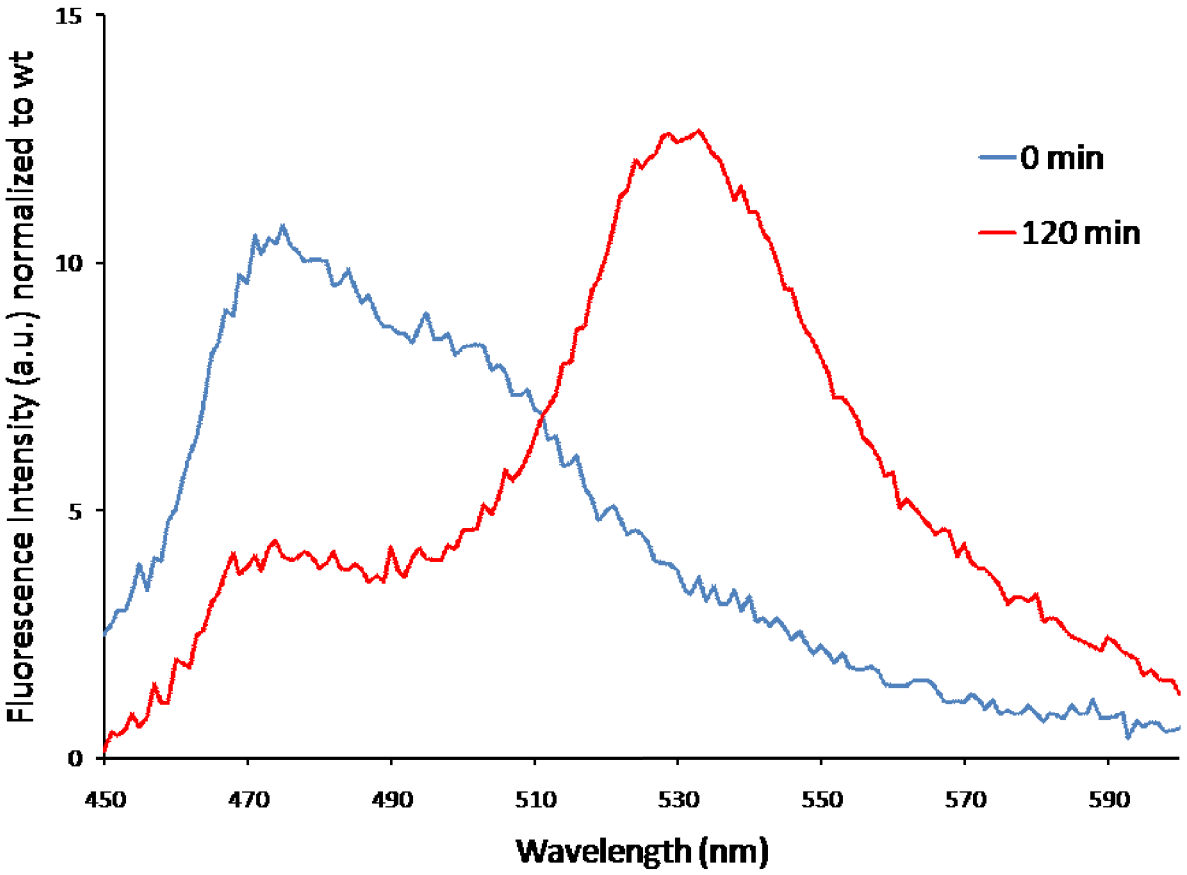

Figure 11. FlAsH-labeling and FRET observation in inverted membrane vesicles of a_ECFP-4Cysγ construct normalized to wt. The graph shows the fluorescence intensity, measured using an excitation wavelength of 434 nm, of a_ECFP- 4Cysγ normalized to wt. Normalization is carried out by subtracting the results of wt from the results of a_ECFP- 4Cysγ. After two hours of FlAsH-labeling, CFP peak at ~475 nm decreased and FlAsH peak at ~530 nm appeared indicating successful FlAsH-labeling and FRET occurrence from CFP to FlAsH.

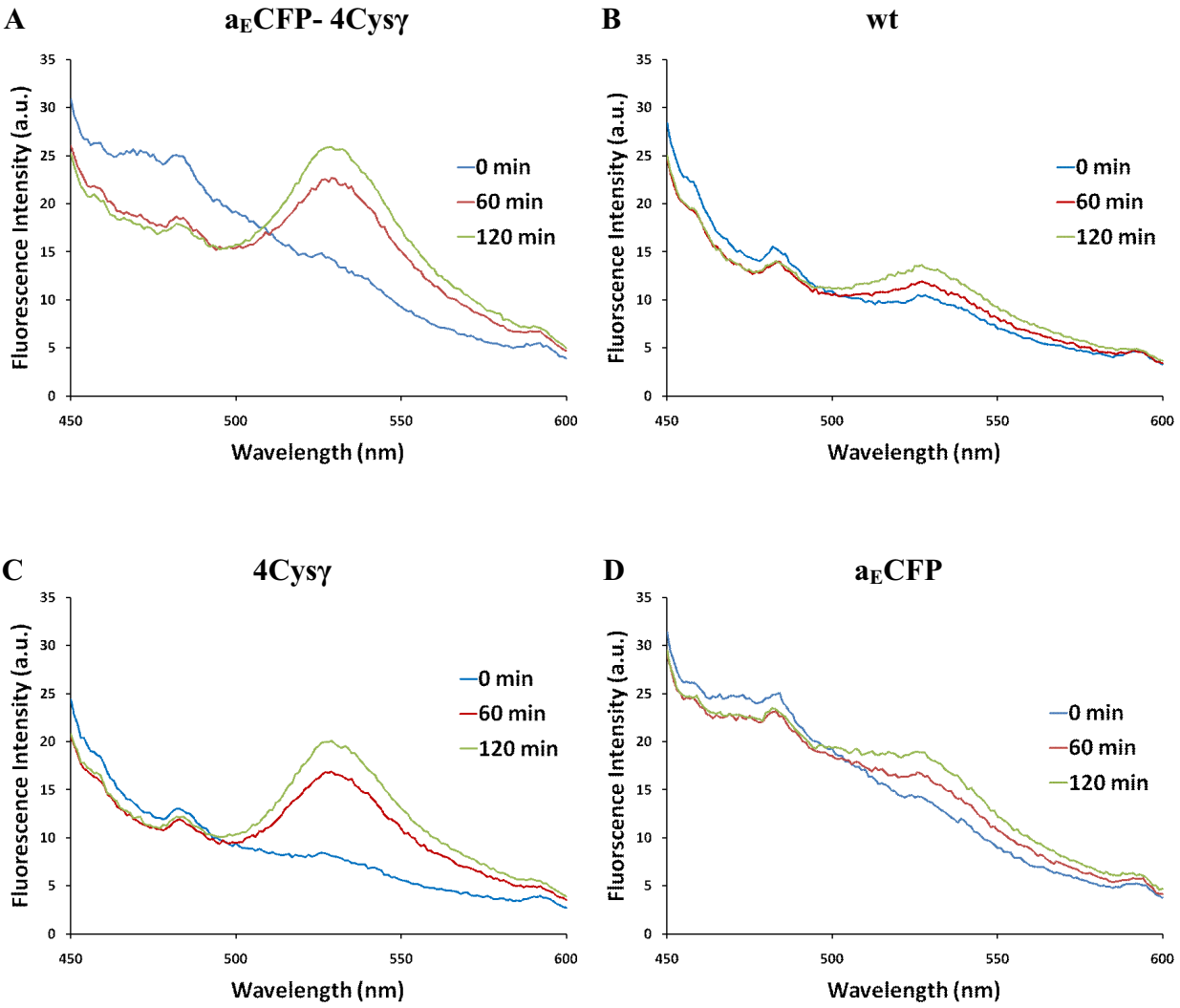

Figure 12. FlAsH-labeling and FRET observation in inverted membrane vesicles of all four constructs. (A) a_ECFP- 4Cysγ (B) wt (C) 4Cysγ (D) a_ECFP. The graphs show the fluorescence intensity of the four constructs at 0, 60 and 120 minutes with the excitation wavelength set at 434 nm (specific for CFP). In a_ECFP- 4Cysγ, after two hours of FlAsH-labeling the CFP peak at ~475 nm decreased and the FlAsH peak at ~530 nm appeared indicating successful FlAsH-labeling and FRET occurrence from CFP to FlAsH. This is not seen in the wt and a_ECFP constructs since they lacked the FlAsH motif. The FlAsH peak in the 4Cysγ construct, which contained the FlAsH motif, increased by time although this construct did not contain CFP. This means that FlAsH can be excited with the 434 nm wavelength which is specific for CFP. Therefore, the increase seen in (A) is not entirely due to FRET but some of it is due to the fact that FlAsH can be slightly excited at 434 nm.

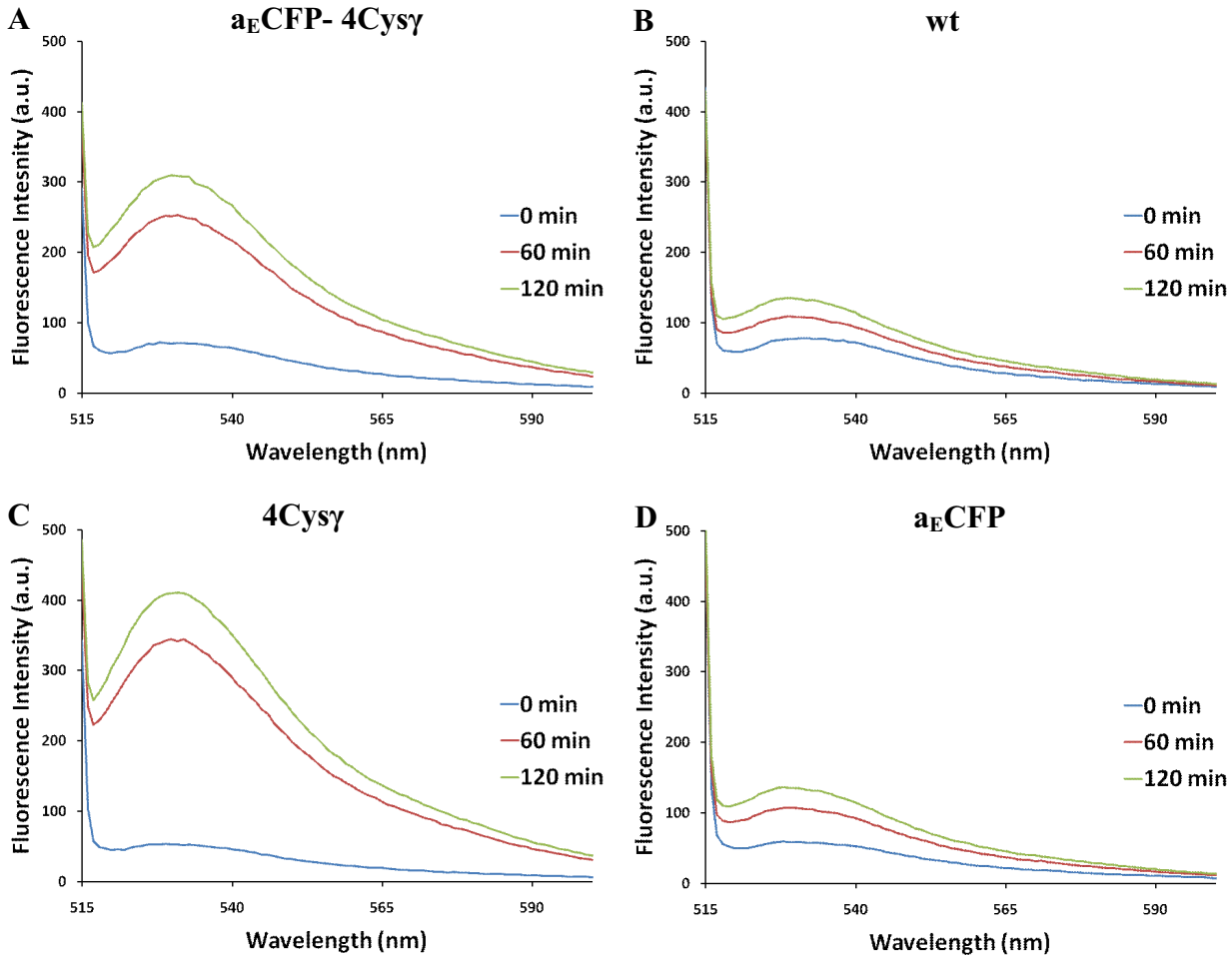

Figure 13. FlAsH peak in inverted membrane vesicles of all four constructs. (A) a_ECFP-4Cysγ (B) wt (C) 4Cysγ (D) a_ECFP. The graphs show the fluorescence intensity of the four constructs at 0, 60 and 120 minutes with the excitation wavelength set at 508 nm (specific for FlAsH). In the a_ECFP- 4Cysγ and 4Cysγ constructs, after two hours, the FlAsH peak at ~530 nm appeared indicating successful FlAsH-labeling. This is not seen in the wt and a_ECFP constructs since they lacked the FlAsH motif.

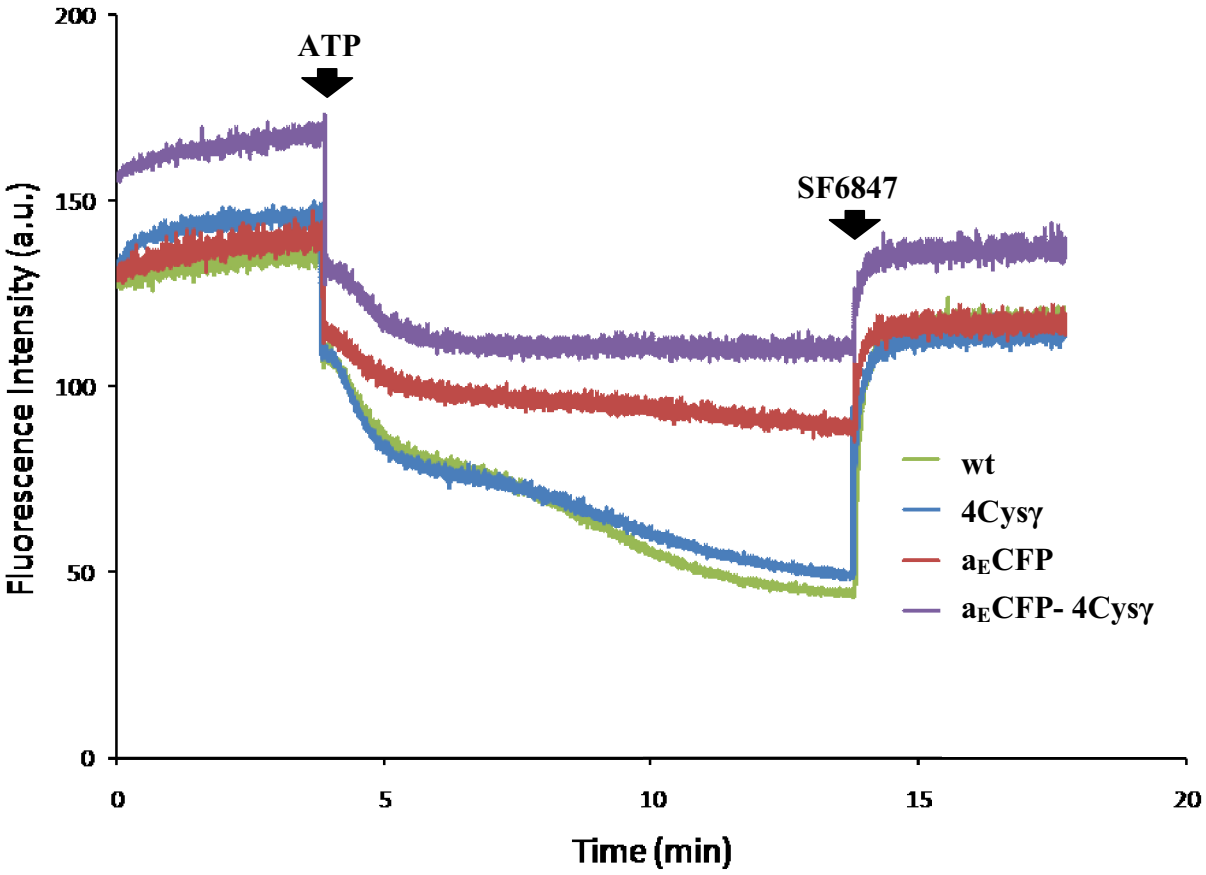

Figure 14. Proton transport measurement in inverted membrane vesicles after FlAsH-labeling. To confirm the functionality of ATP synthase in all four constructs after two hours of FlAsH-labeling, proton transport was monitored by fluorescence quenching of ACMA, as described previously in Figure 10. The graph shows that all four constructs were still active.

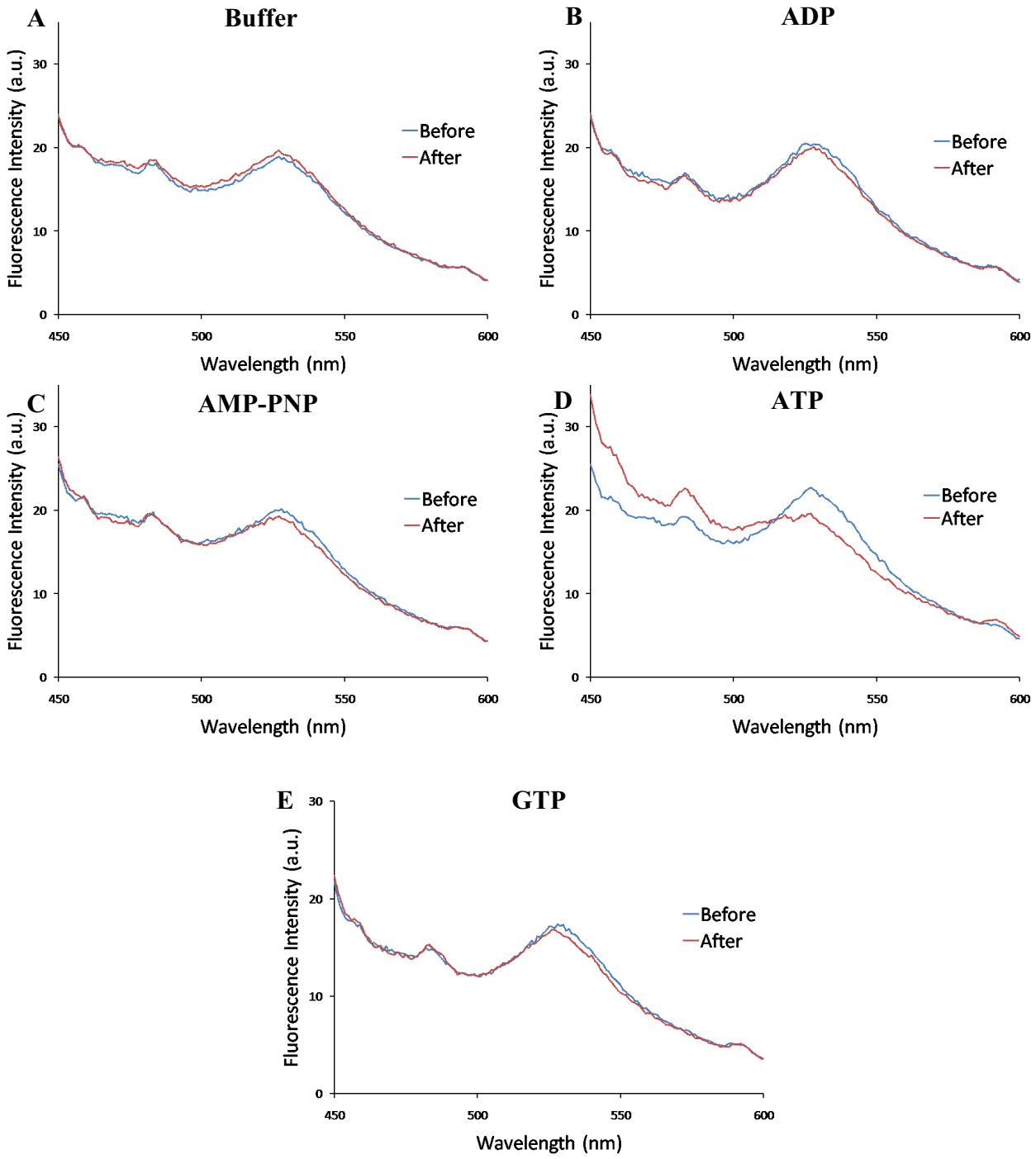

Figure 15. Nucleotide-dependency of FRET signal in a_ECFP- 4Cysγ construct. The graphs show the FRET signal with the excitation wavelength set at 434 nm before and after the addition of 20 µL of 100 mM of each nucleotide to achieve a final concentration of 2 mM. Nucleotides were added after two hours of FlAsH-labeling. I_D/I_A was calculated for each case with the donor peak at 475 nm and the acceptor peak at 528 nm. (A) 20 µL of buffer PA4. I_D/I_A before and after addition of buffer = 0.93 (B) ADP: $[I_D/I_A]_{Before} = 0.91$, $[I_D/I_A]_{After} = 0.96$ (C) AMP-PNP: $[I_D/I_A]_{Before} = 0.79$, $[I_D/I_A]_{After} = 0.77$ (D) ATP: $[I_D/I_A]_{Before} = 0.81$, $[I_D/I_A]_{After} = 1.10$. (E) GTP: $[I_D/I_A]_{Before} = 0.82$, $[I_D/I_A]_{After} = 0.86$. The graphs show that ATP causes a significant change in the FRET signal.

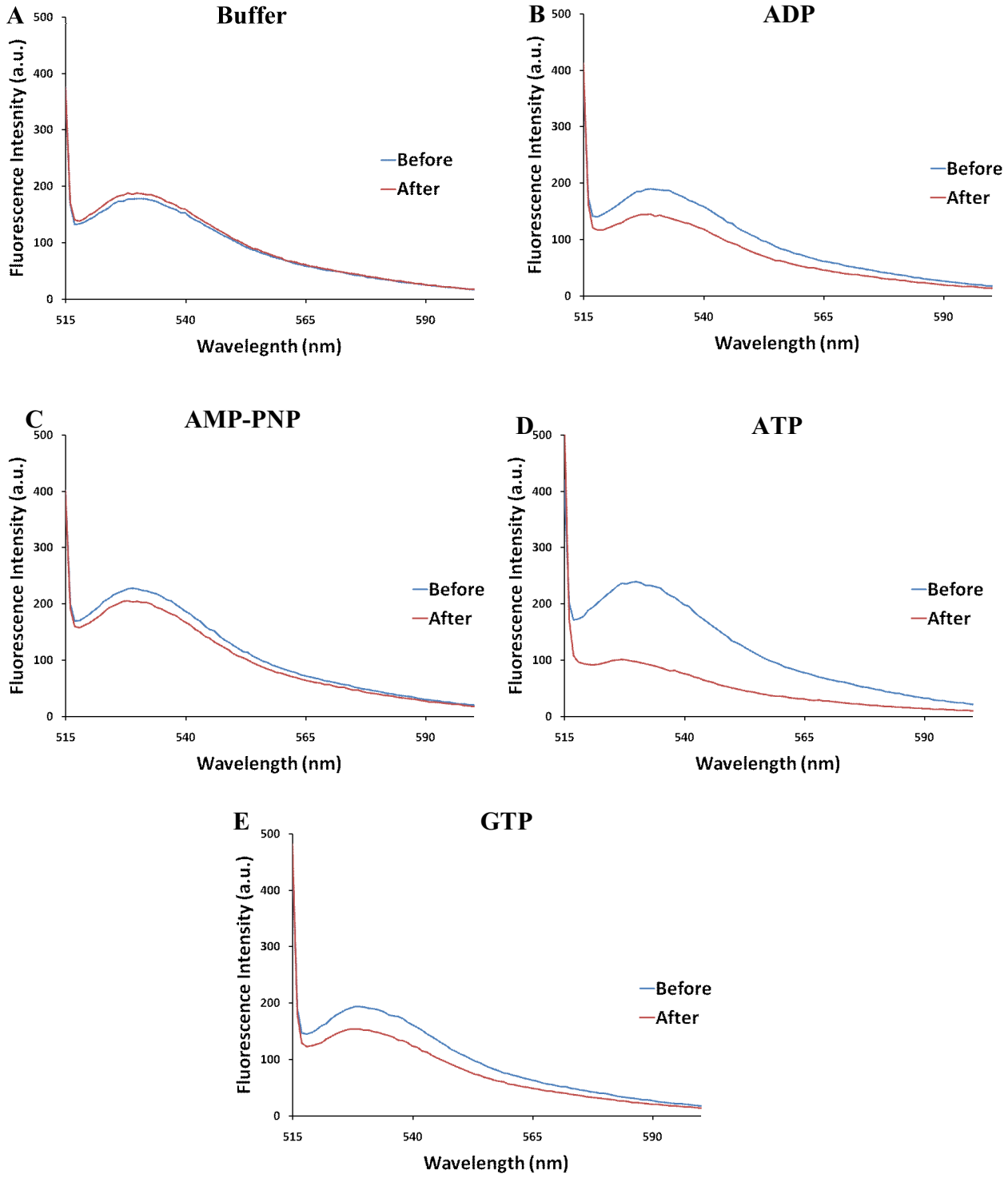

Figure 16. Nucleotide-dependency of FlAsH signal in a_ECFP- 4Cysγ construct. The graphs show the FlAsH peak with the excitation wavelength set at 508 nm before and after the addition of 20 µL of 100 mM of each nucleotide to achieve a final concentration of 2 mM. Nucleotides were added after two hours of FlAsH-labeling. (A) 20 µL of buffer PA4 (B) ADP (C) AMP-PNP (D) ATP (E) GTP. A significant decrease in the FlAsH peak is observed with ATP as opposed to the buffer and the other nucleotides.

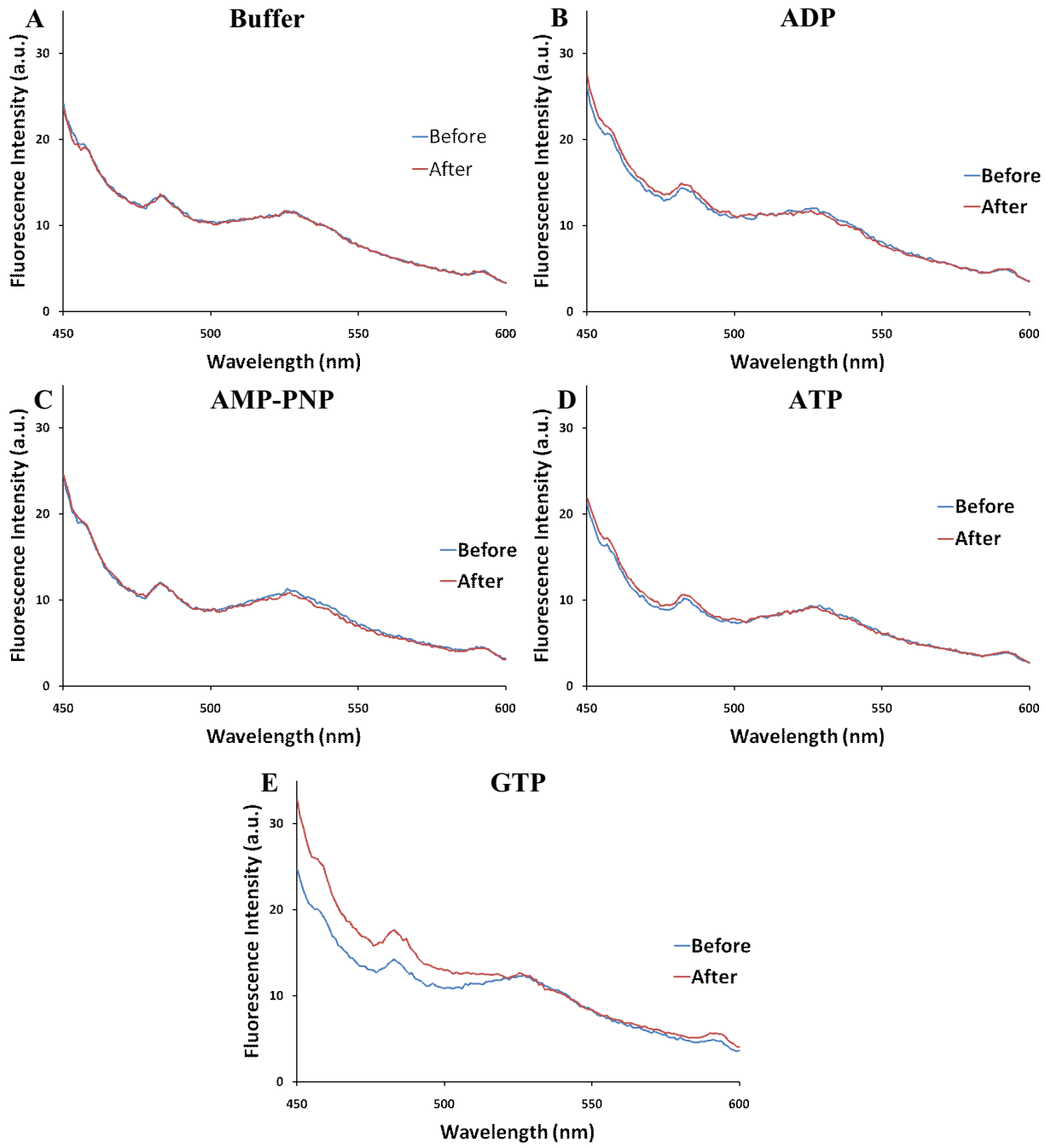

Figure 17. Nucleotide-dependency of FRET signal in wt construct. The graphs show the FRET signal with the excitation wavelength set at 434 nm before and after the addition of 20 µL of 100 mM of each nucleotide to achieve a final concentration of 2 mM. Nucleotides were added after two hours of FlAsH-labeling. I_D/I_A was calculated for each case with the donor peak at 475 nm and the acceptor peak at 528 nm. (A) 20 µL of buffer PA4. Before and after addition of buffer, I_D/I_A = 1.07 (B) ADP: $[I_D/I_A]_{Before}$ = 1.11, $[I_D/I_A]_{After}$ = 1.22 (C) AMP-PNP: $[I_D/I_A]_{Before}$ = 0.94, $[I_D/I_A]_{After}$ = 1.02 (D) ATP: $[I_D/I_A]_{Before}$ = 1.07, $[I_D/I_A]_{After}$ = 1.32 (E) GTP: $[I_D/I_A]_{Before}$ = 0.98, $[I_D/I_A]_{After}$ = 1.02. The graphs show that ATP causes a change in the FRET signal.

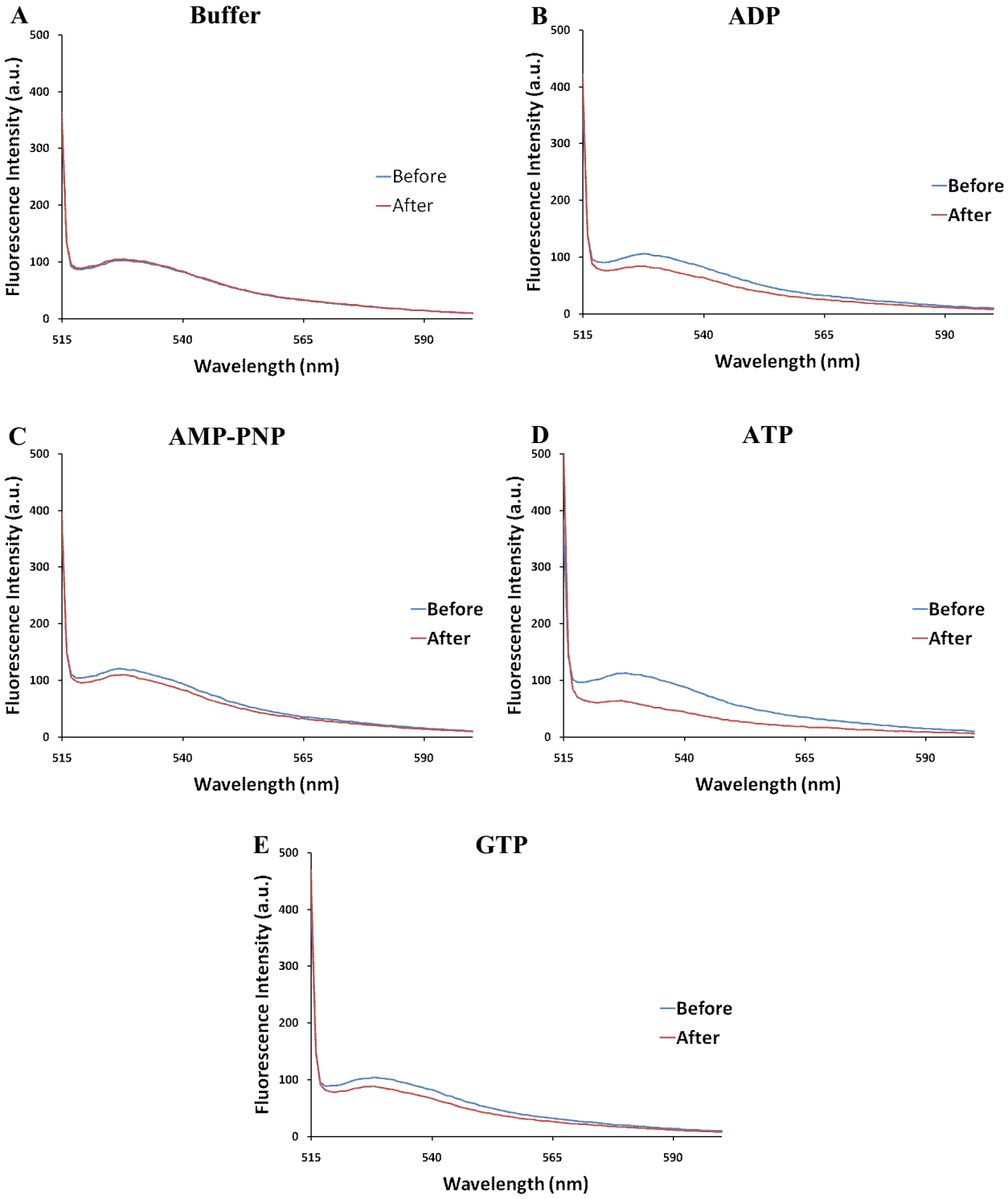

Figure 18. Nucleotide-dependency of FlAsH signal in wt construct. The graphs show the FlAsH peak with the excitation wavelength set at 508 nm before and after the addition of 20 µL of 100 mM of each nucleotide to achieve a final concentration of 2 mM. Nucleotides were added after two hours of FlAsH-labeling. (A) 20 µL of buffer PA4 (B) ADP (C) AMP-PNP (D) ATP (E) GTP.

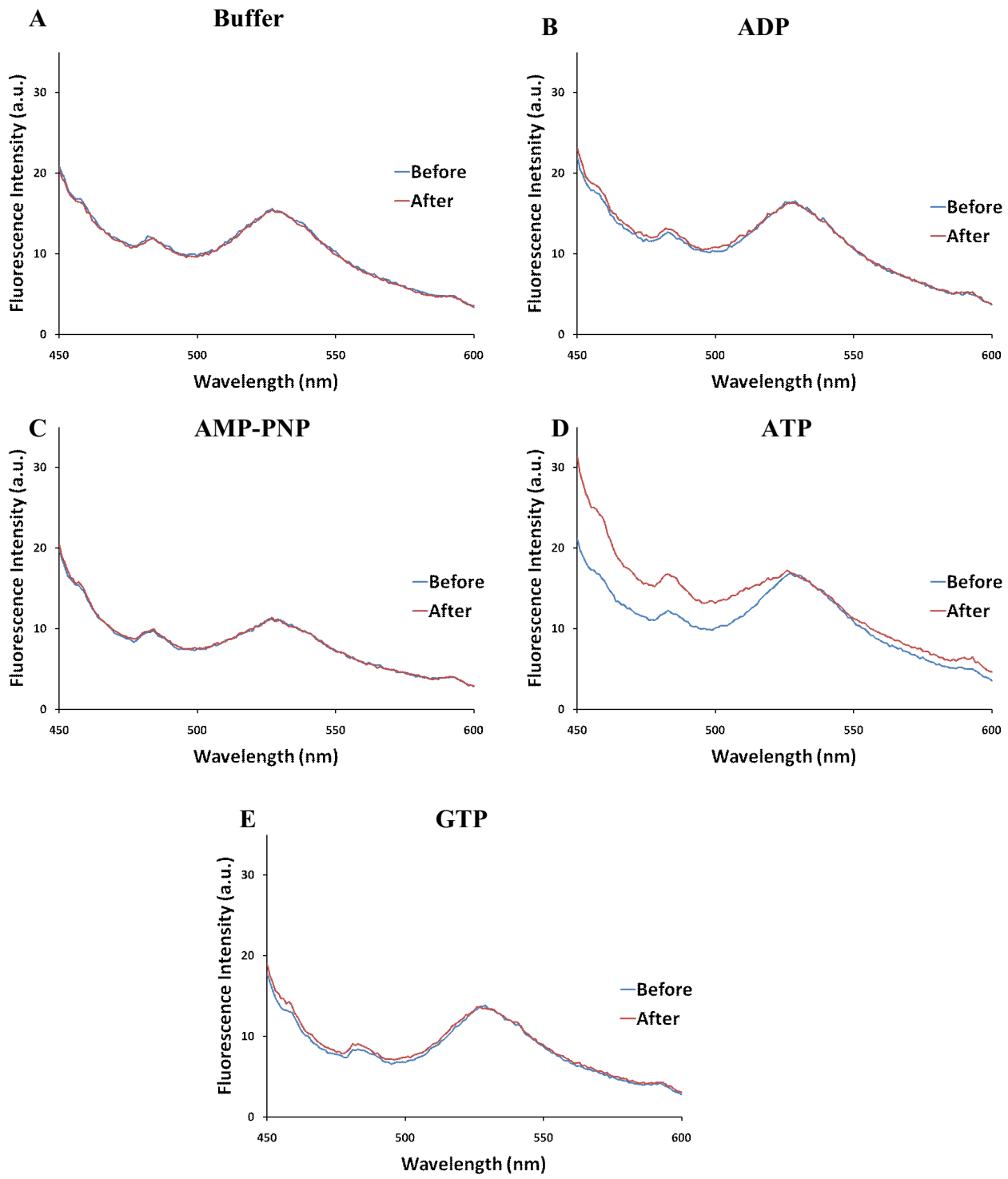

Figure 19. Nucleotide-dependency of FRET signal in 4Cysγ construct. The graphs show the FRET signal with the excitation wavelength set at 434 nm before and after the addition of 20 µL of 100 mM of each nucleotide to achieve a final concentration of 2 mM. Nucleotides were added after two hours of FlAsH-labeling. I_D/I_A was calculated for each case with the donor peak at 475 nm and the acceptor peak at 528 nm. (A) 20 µL of buffer PA4: $[I_D/I_A]_{Before} = 0.73$ $[I_D/I_A]_{After} = 0.72$ (B) ADP: $[I_D/I_A]_{Before} = 0.72$, $[I_D/I_A]_{After} = 0.76$ (C) AMP-PNP: $[I_D/I_A]_{Before} = 0.79$, $[I_D/I_A]_{After} = 0.81$ (D) ATP: $[I_D/I_A]_{Before} = 0.69$, $[I_D/I_A]_{After} = 0.93$ (E) GTP: $[I_D/I_A]_{Before} = 0.57$, $[I_D/I_A]_{After} = 0.60$. The graphs show that ATP causes a change in the FRET signal.

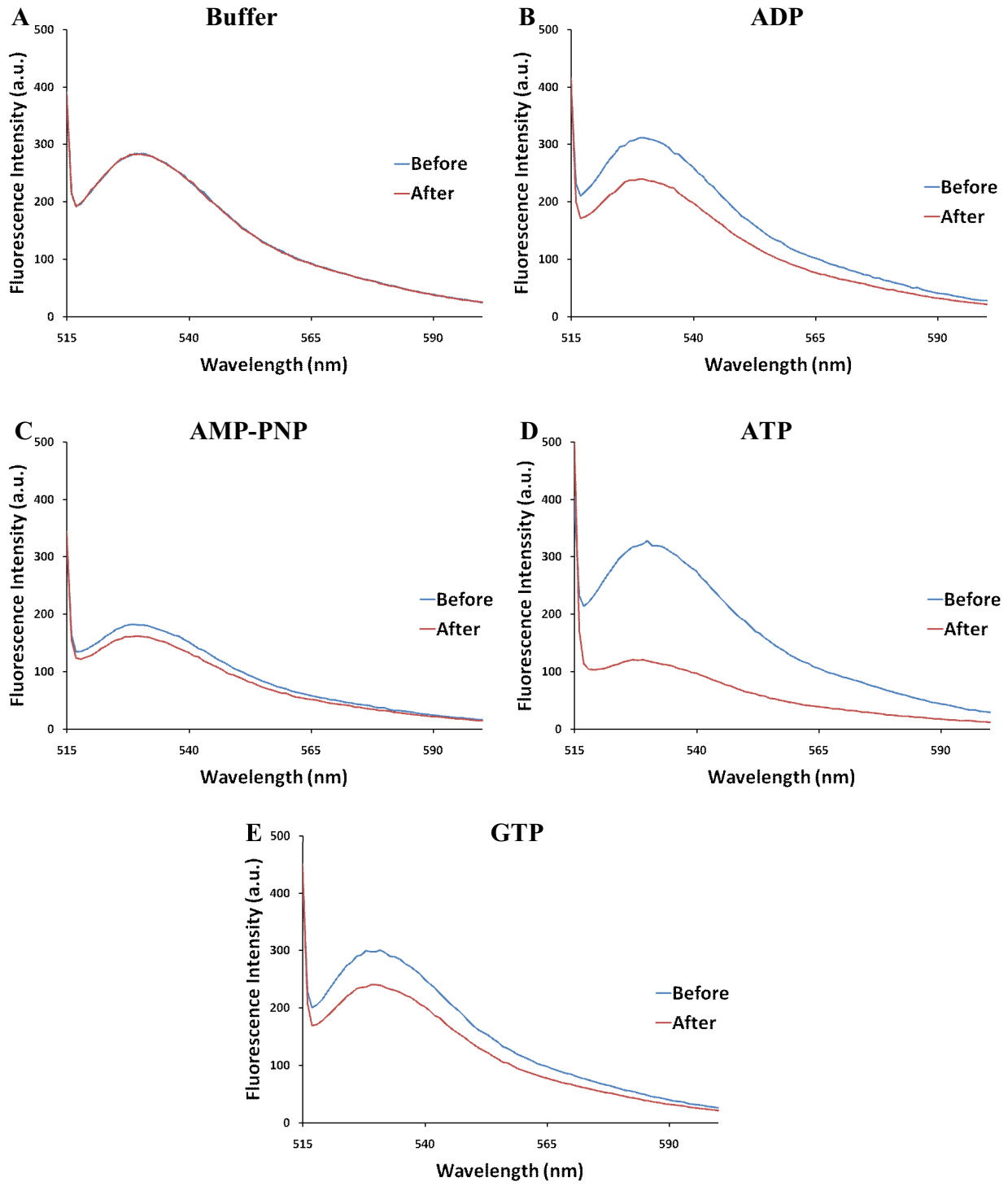

Figure 20. Nucleotide-dependency of FlAsH signal in 4Cysγ construct. The graphs show the FlAsH peak with the excitation wavelength set at 434 nm before and after the addition of 20 µL of 100 mM of each nucleotide to achieve a final concentration of 2 mM. Nucleotides were added after two hours of FlAsH-labeling. (A) 20 µL of buffer PA4 (B) ADP (C) AMP-PNP (D) ATP (E) GTP. A significant decrease in the FlAsH peak is observed with ATP.

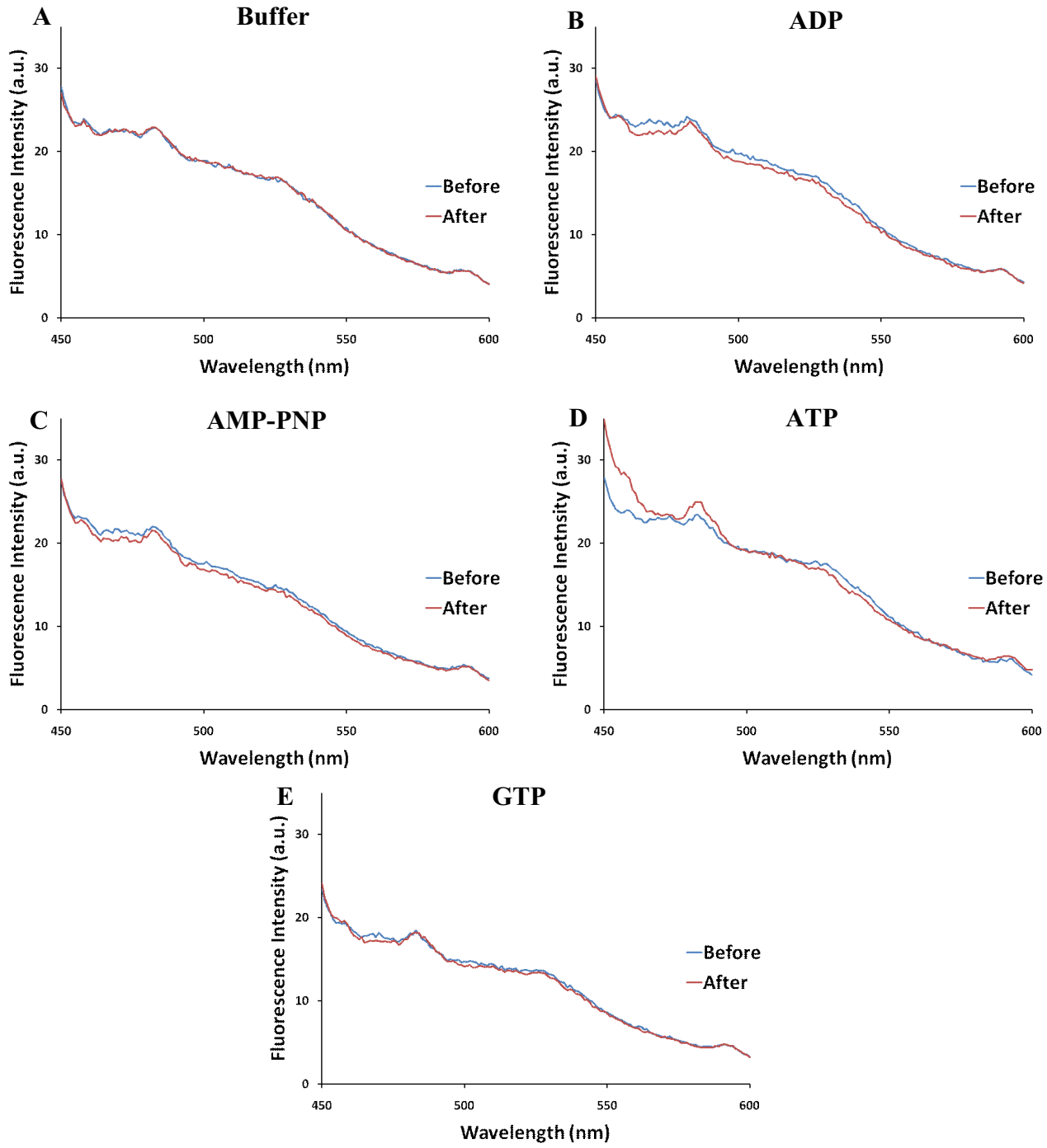

Figure 21. Nucleotide-dependency of FRET signal in a_ECFP construct. The graphs show the FRET signal with the excitation wavelength set at 434 nm before and after the addition of 20 µL of 100 mM of each nucleotide to achieve a final concentration of 2 mM. Nucleotides were added after two hours of FlAsH-labeling. I_D/I_A was calculated for each case with the donor peak at 475 nm and the acceptor peak at 528 nm. (A) 20 µL of buffer PA4: $[I_D/I_A]_{Before} = 1.35$ $[I_D/I_A]_{After} = 1.36$ (B) ADP: $[I_D/I_A]_{Before} = 1.40$, $[I_D/I_A]_{After} = 1.37$ (C) AMP-PNP: $[I_D/I_A]_{Before} = 1.47$, $[I_D/I_A]_{After} = 1.43$ (D) ATP: $[I_D/I_A]_{Before} = 1.29$, $[I_D/I_A]_{After} = 1.38$ (E) GTP: $[I_D/I_A]_{Before} = 1.29$, $[I_D/I_A]_{After} = 1.30$. The graphs show that ATP causes a slight change in the FRET signal.

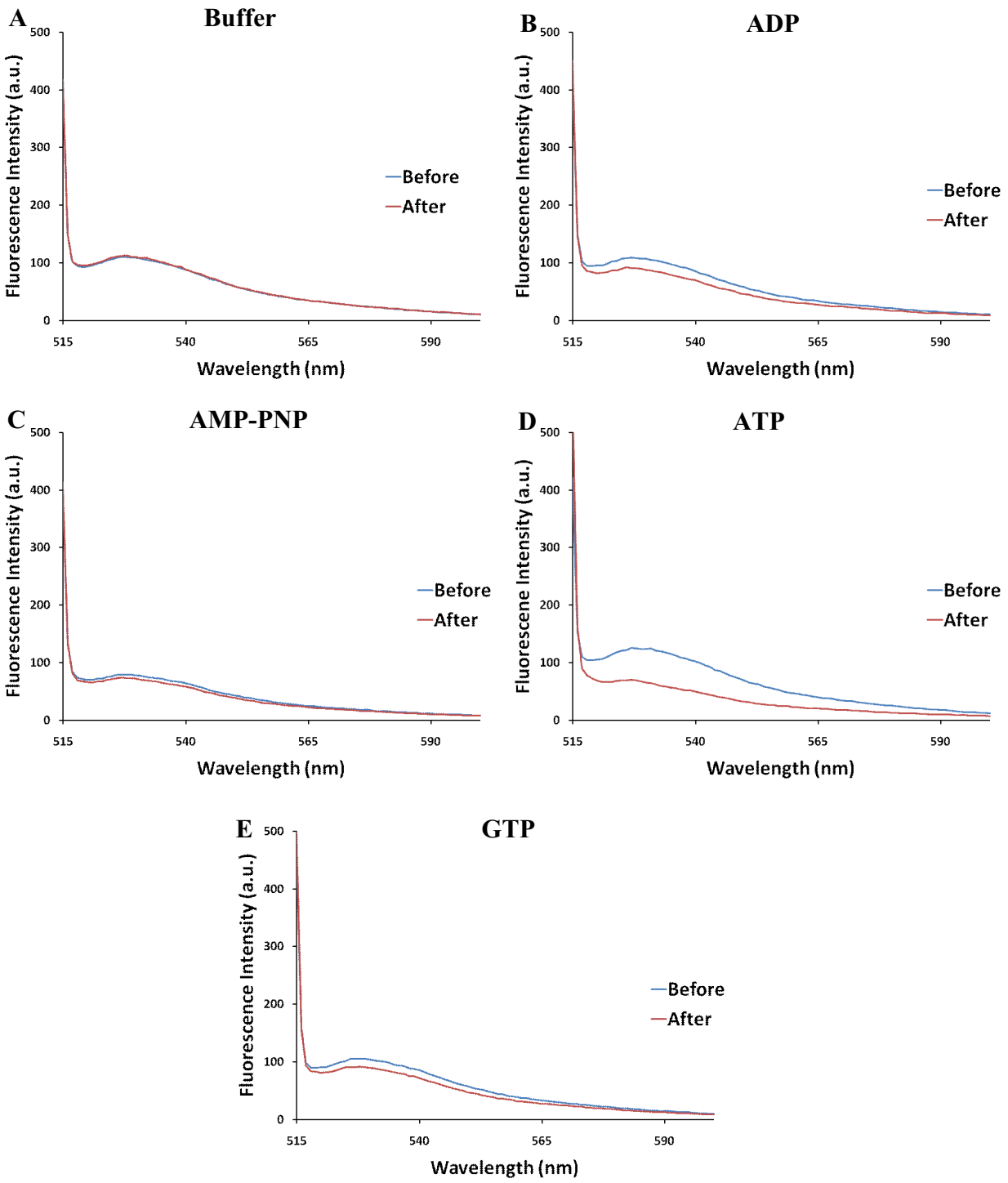

Figure 22. Nucleotide-dependency of FlAsH signal in a_ECFP construct. The graphs show the FlAsH peak with the excitation wavelength set at 434 nm before and after the addition of 20 µL of 100 mM of each nucleotide to achieve a final concentration of 2 mM. Nucleotides were added after two hours of FlAsH-labeling. (A) 20 µL of buffer PA4 (B) ADP (C) AMP-PNP (D) ATP (E) GTP.

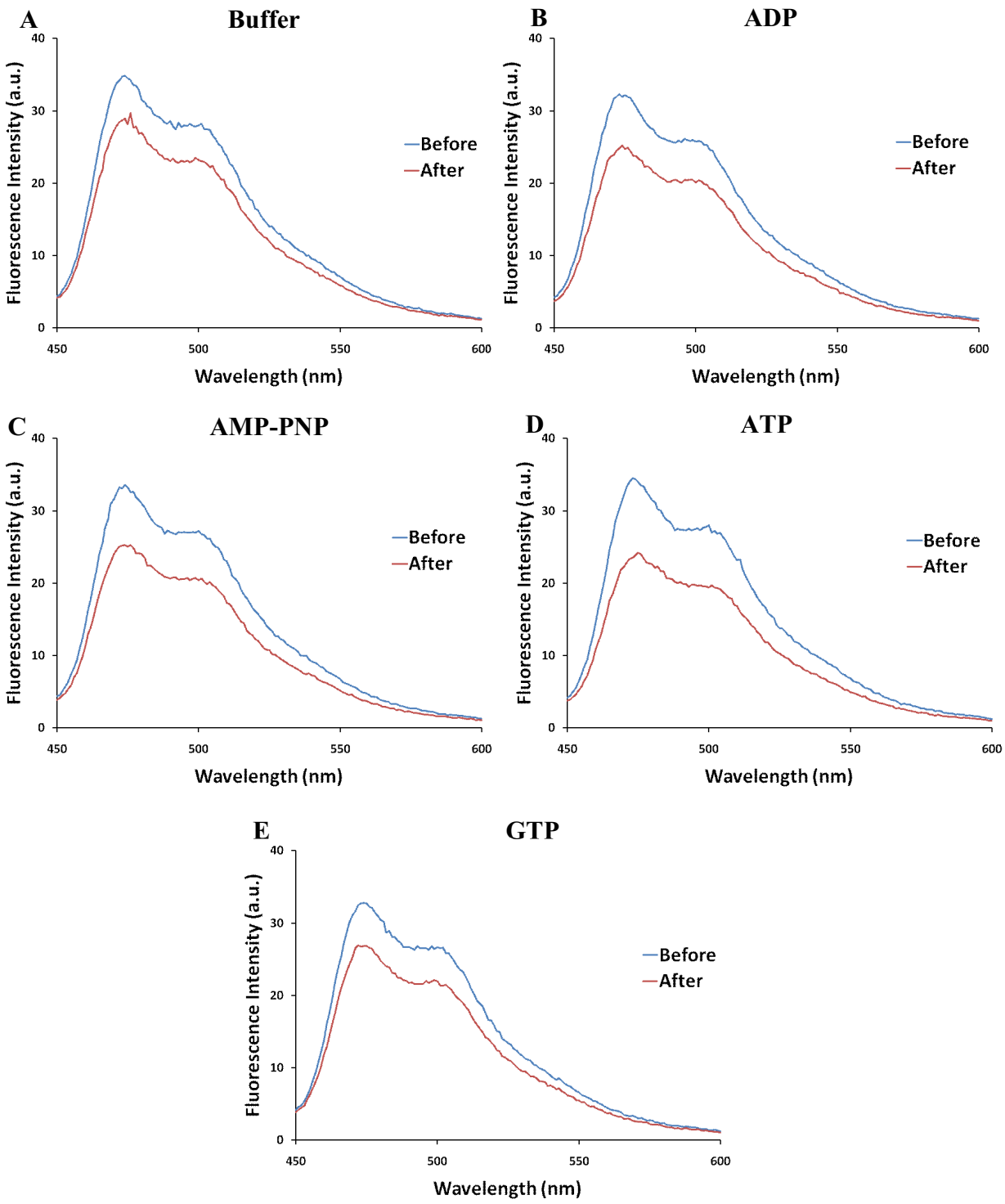

Figure 23. Effect of addition of 2 mM nucleotides on CFP. The graphs show the CFP signal (excitation at 434 nm) before and after the addition of 20 µL of 100 mM of each nucleotide to achieve a final concentration of 2 mM. (A) 20 µL of buffer PA4, ~ 19% quenching (B) ADP, ~ 25% quenching (C) AMP-PNP, ~ 25% quenching (D) ATP, ~ 29% quenching (E) GTP, ~ 18% quenching. The graphs show that ATP causes a greater degree of CFP quenching than the other nucleotides.

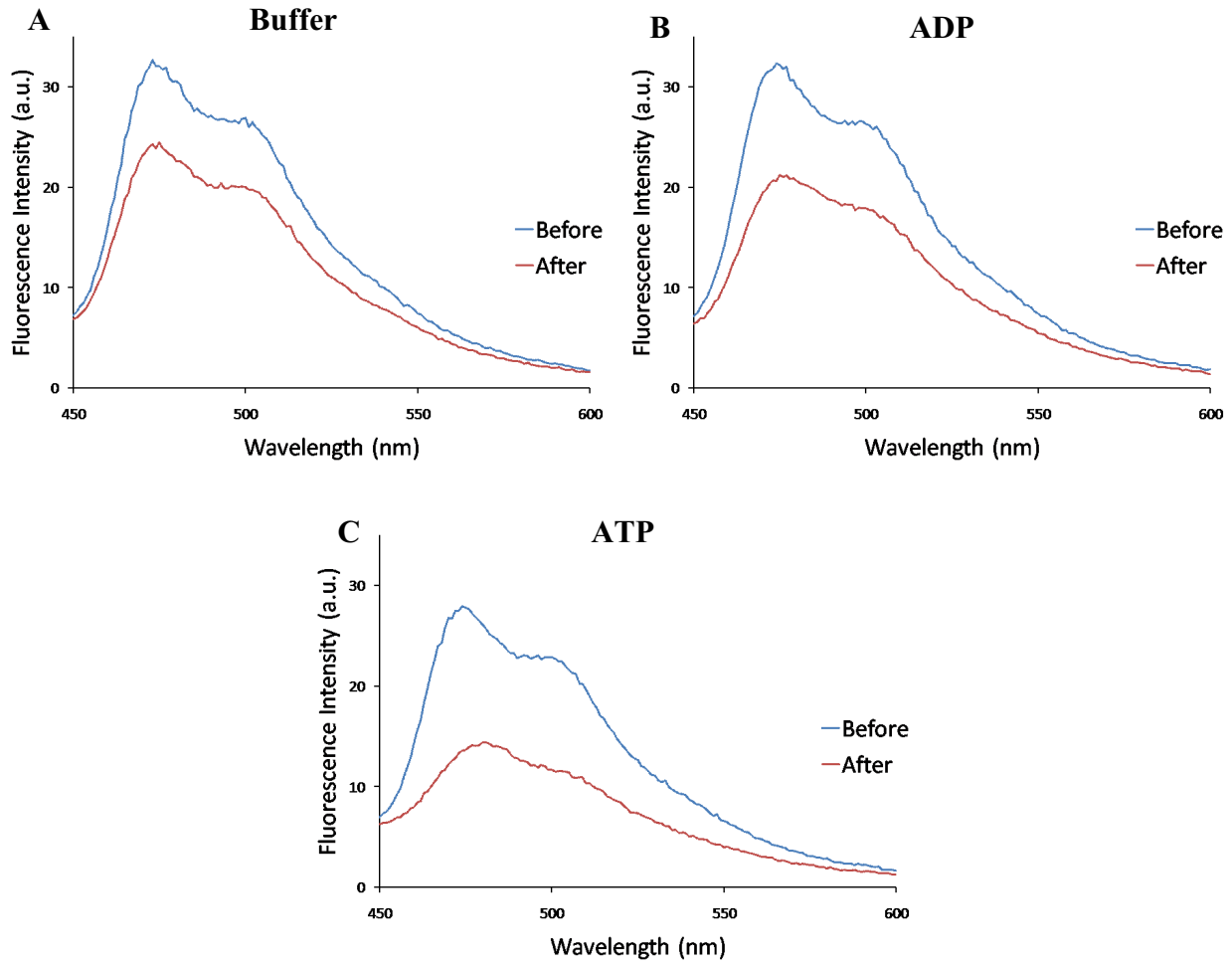

Figure 24. Effect of addition of 10 mM nucleotides on CFP. The graphs show the CFP signal (excitation at 434 nm) before and after the addition of 100 µL of 100 mM of each nucleotide to achieve a final concentration of 10 mM. (A) 100 µL of buffer PA4 showing ~25% quenching (B) ADP showing ~34% quenching (C) ATP showing ~50% quenching. The graphs show that ATP has a greater quenching effect on CFP compared to ADP and the buffer.

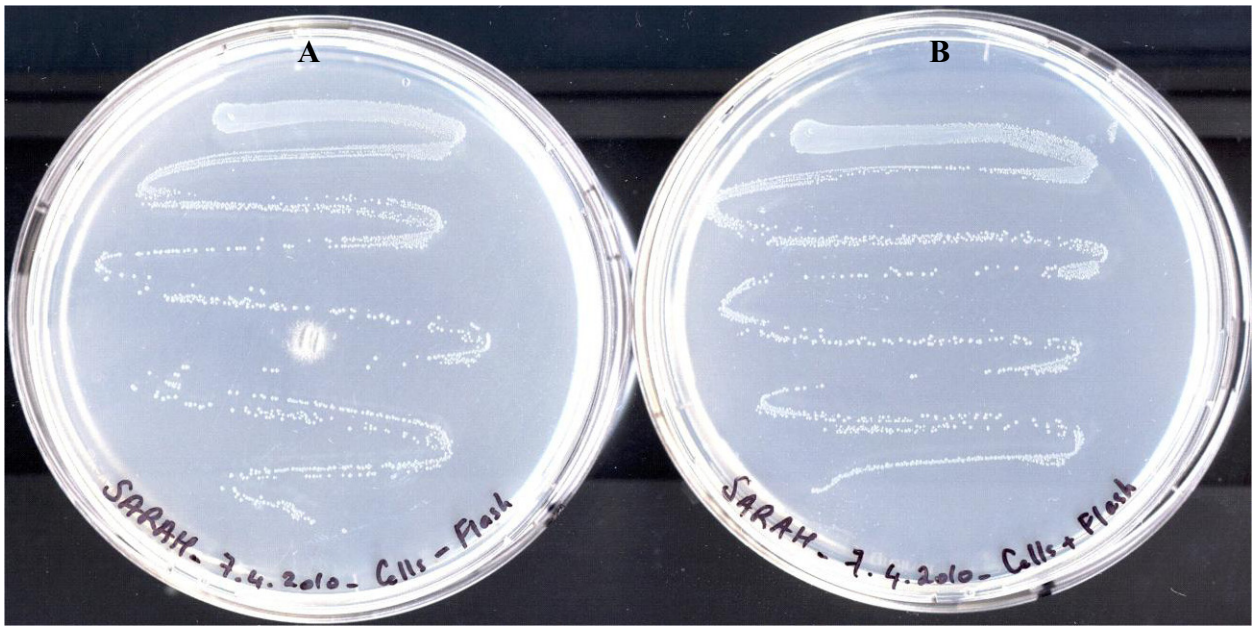

Figure 25. Effect of FlAsH-EDT$_2$ on cell survival. 50 µL of FlAsH-EDT$_2$ was added to a solution containing whole cells and 50 µL of buffer PA4 to another solution containing the same volume of whole cells. After ~3 hours, ~3 µL of each sample was streaked on a plate and plates were left overnight in an incubator at 37 °C. (A) Whole cells without FlAsH-labeling (B) Whole cells with FlAsH-labeling. The picture shows no significant difference in the number of cells between the two samples indicating that FlAsH did not affect cell survival.

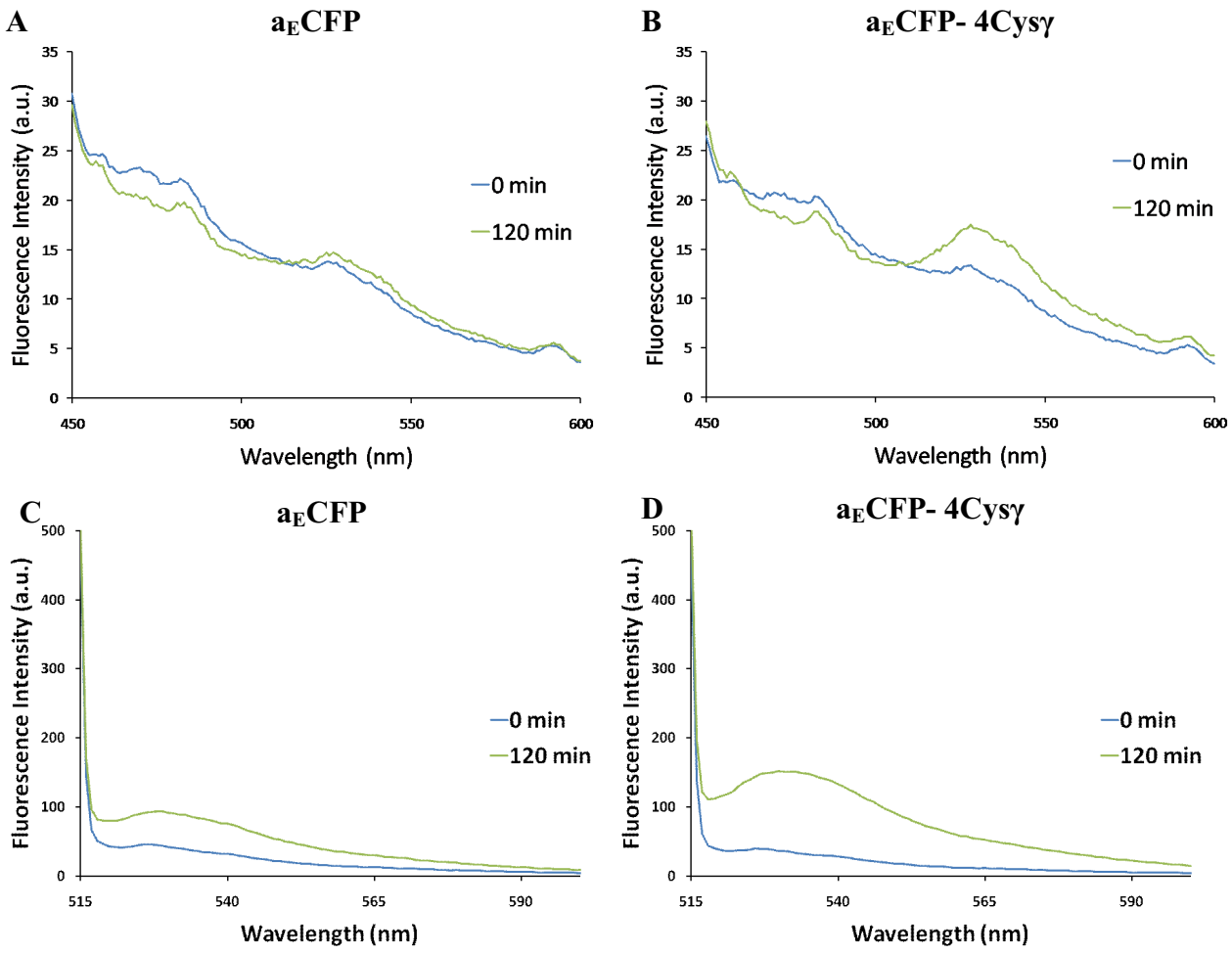

Figure 26. FlAsH-labeling and FRET observation in whole cells. The graph shows the fluorescence intensity of whole cells at 434 and 508 nm. (A) a_ECFP at 434 nm. (B) a_ECFP-4Cysγ at 434 nm. After two hours of FlAsH-labeling, CFP peak at ~475 nm decreased and FlAsH peak at ~530 nm appeared indicating successful FlAsH-labeling and the possibility of FRET occurrence from CFP to FlAsH. (C) a_ECFP at 508 nm. (D) a_ECFP- 4Cysγ at 508 nm. The FlAsH peak significantly increases with time indicating successful FlAsH-labeling.

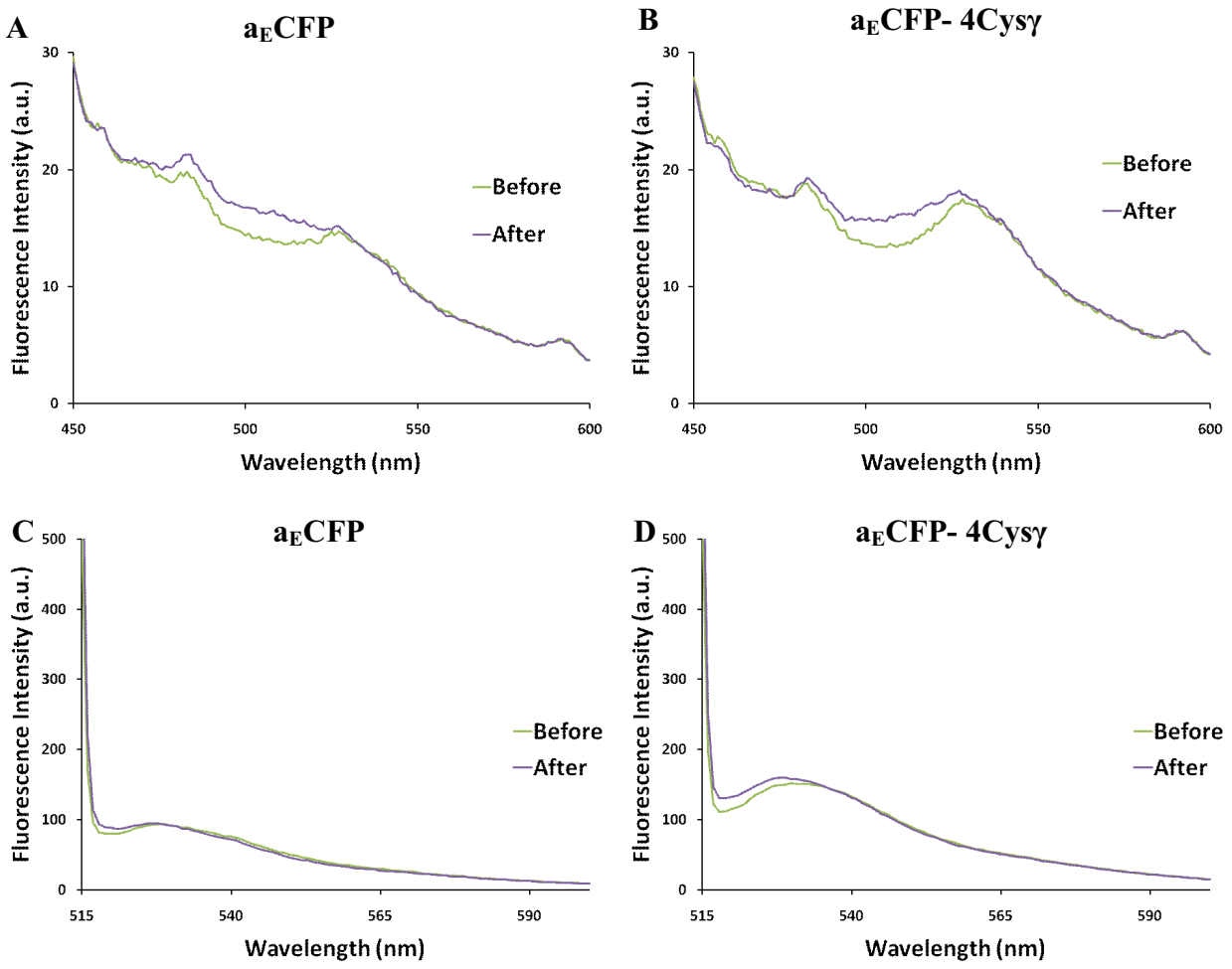

Figure 27. Effect of addition of ATP on FRET signal in whole cells. After two hours of FlAsH-labeling, 20 µL of 100 mM ATP was added to achieve a final concentration of 2 mM (A) a_ECFP at 434 nm: $[I_D/I_A]_{Before} = 1.34$, $[I_D/I_A]_{After} = 1.35$ (B) a_ECFP- 4Cysγ at 434 nm: $[I_D/I_A]_{Before} = 1.02$, $[I_D/I_A]_{After} = 0.99$ (C) a_ECFP at 508 nm (D) a_ECFP- 4Cysγ at 508 nm. The graphs show no significant change in the FRET signal or the FlAsH peak upon addition of ATP.

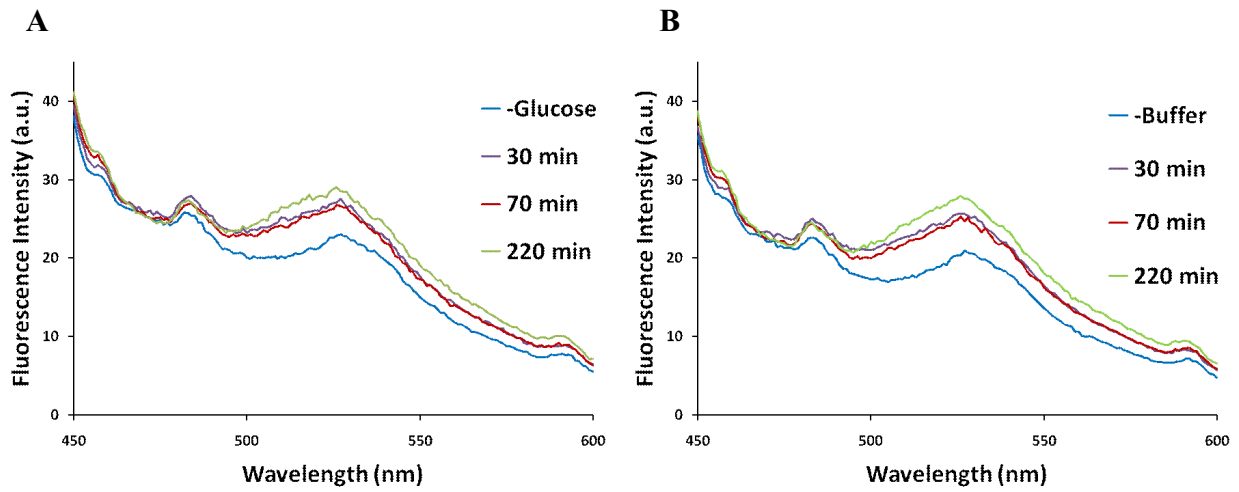

Figure 28. Effect of incubation with glucose on FRET signal in whole cells. After two hours of FlAsH-labeling, 25 µL of 1 M glucose was added to one sample to achieve a final concentration of 25 mM and 25 µL of buffer PA4 was added to another sample as a control. Both samples were incubated at 37°C and the signal was measured after 30, 70 and 220 min. (A) Before and after the addition of glucose using an excitation wavelength of 434 nm (B) Before and after the addition of buffer PA4 using an excitation wavelength of 434 nm. In spite of the increase in the FlAsH peak by time, the graphs show no difference between the addition of glucose and buffer PA4.

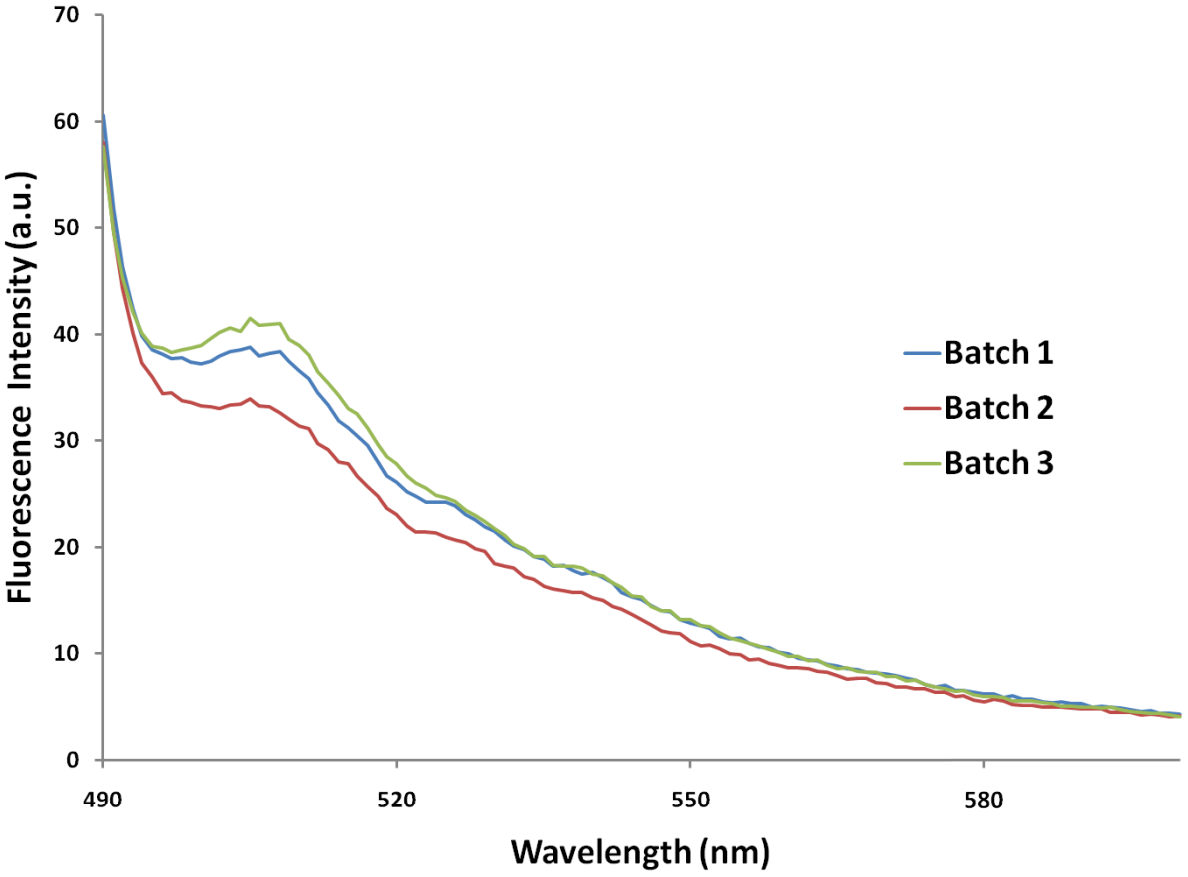

Figure 29. GFP fluorescence detection. The graph shows the fluorescence intensity of three different batches of inverted membrane vesicles of *E. coli* RA1 strain harboring the plasmid pSD166 which codes for *E. coli* ATP synthase with EGFP fused to the C-terminus of the a-subunit of the enzyme. Excitation wavelength was set at 480 nm. The graph shows the maximum peak of GFP (at ~506 nm) present in all three batches.

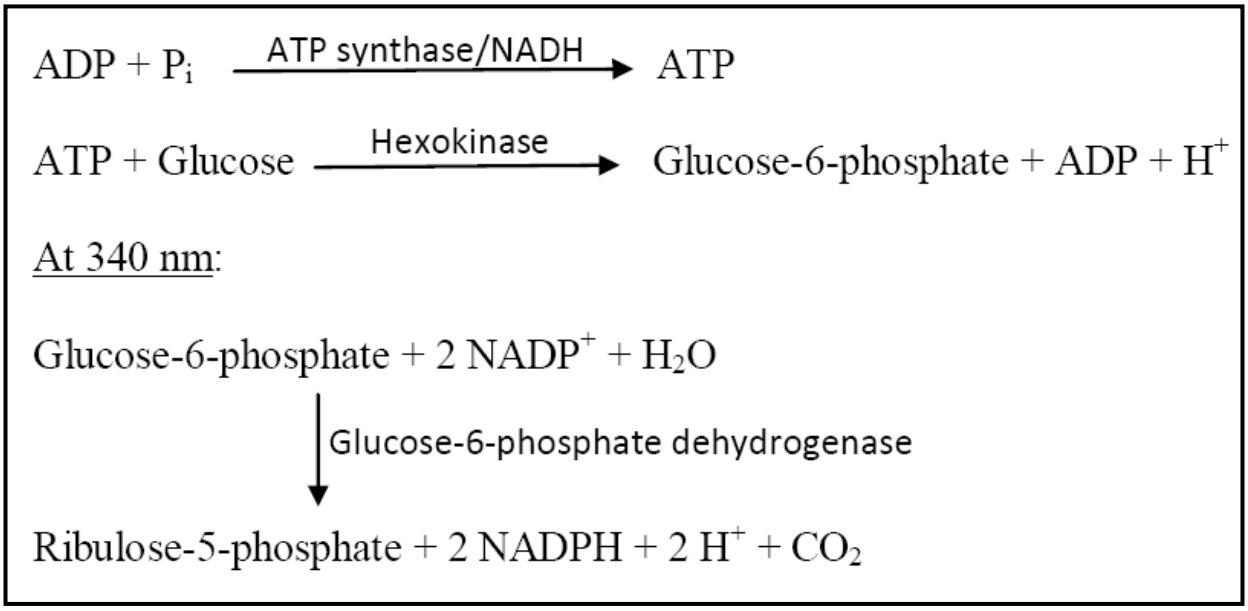

Figure 30. Reactions of the ATP synthesis assay. ATP synthase synthesizes ATP from ADP and inorganic phosphate (P_i) in the presence of NADH. The produced ATP is transformed into glucose-6-phosphate in the presence of hexokinase and glucose in the reaction sample. NADPH is produced upon the addition of glucose-6-phosphate dehydrogenase. The production of NADPH can be monitored at a wavelength of 340 nm.

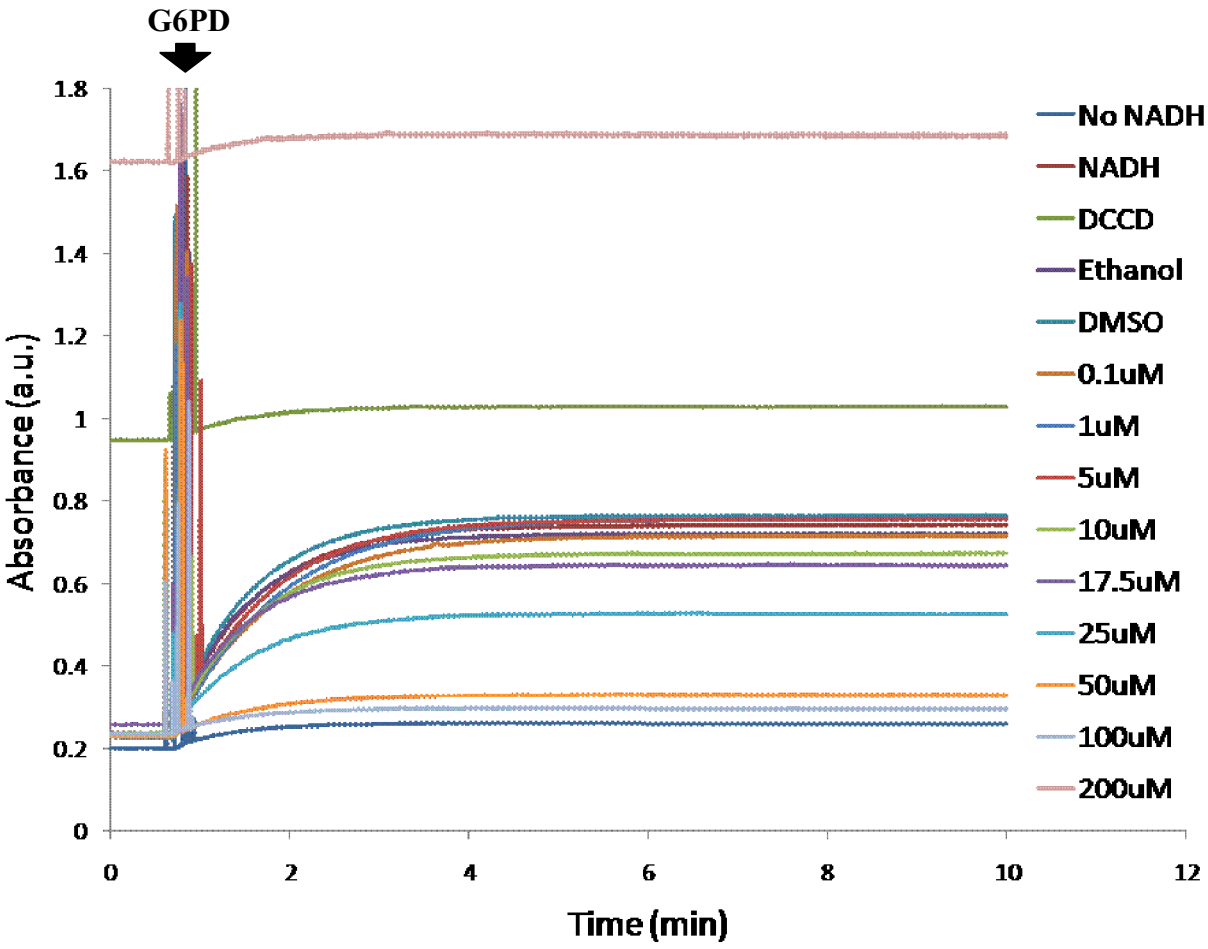

Figure 31. ATP synthesis in inverted membrane vesicles of *E. coli* RA1 strain. The graph represents raw data of one experiment of ATP synthesis using batch 1 and different concentrations of compound 1. Samples were incubated for 20 minutes at 37°C in the presence of NADH, ADP and P_i. The produced ATP is converted to glucose-6-phosphate in the presence of glucose and hexokinase in the reaction sample. Production of NADPH was initiated by the addition of glucose-6-phosphate dehydrogenase (G6PD) and absorbance of NADPH was measured at 340 nm.

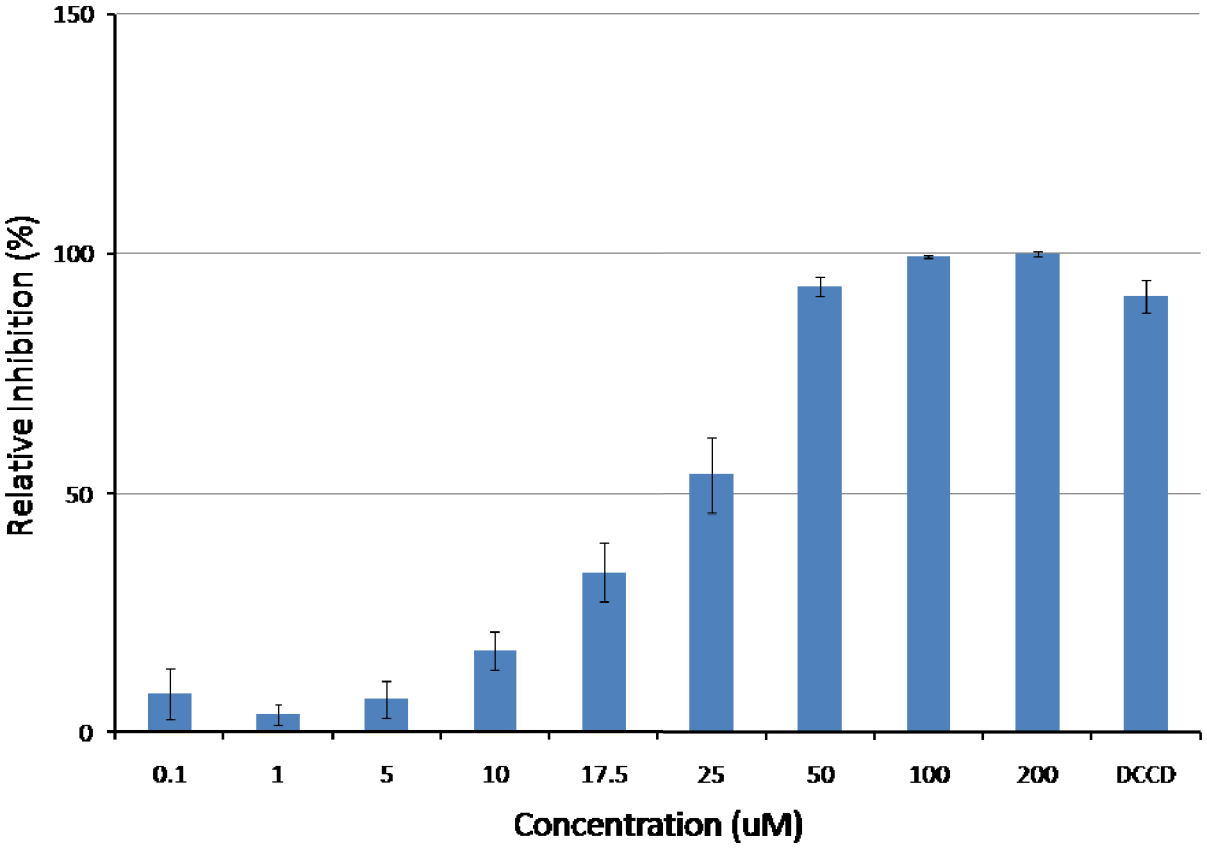

Figure 32. Effect of compound 1 on ATP synthesis in inverted membrane vesicles of *E. coli* RA1 strain using MOPS buffer. The graph represents the mean values of three independent experiments with standard deviation. Inhibition of compound 1 was normalized against DMSO while DCCD was normalized against ethanol. Compound 1 displayed dose-dependent inhibition with an IC_{50} of ~25 μM.

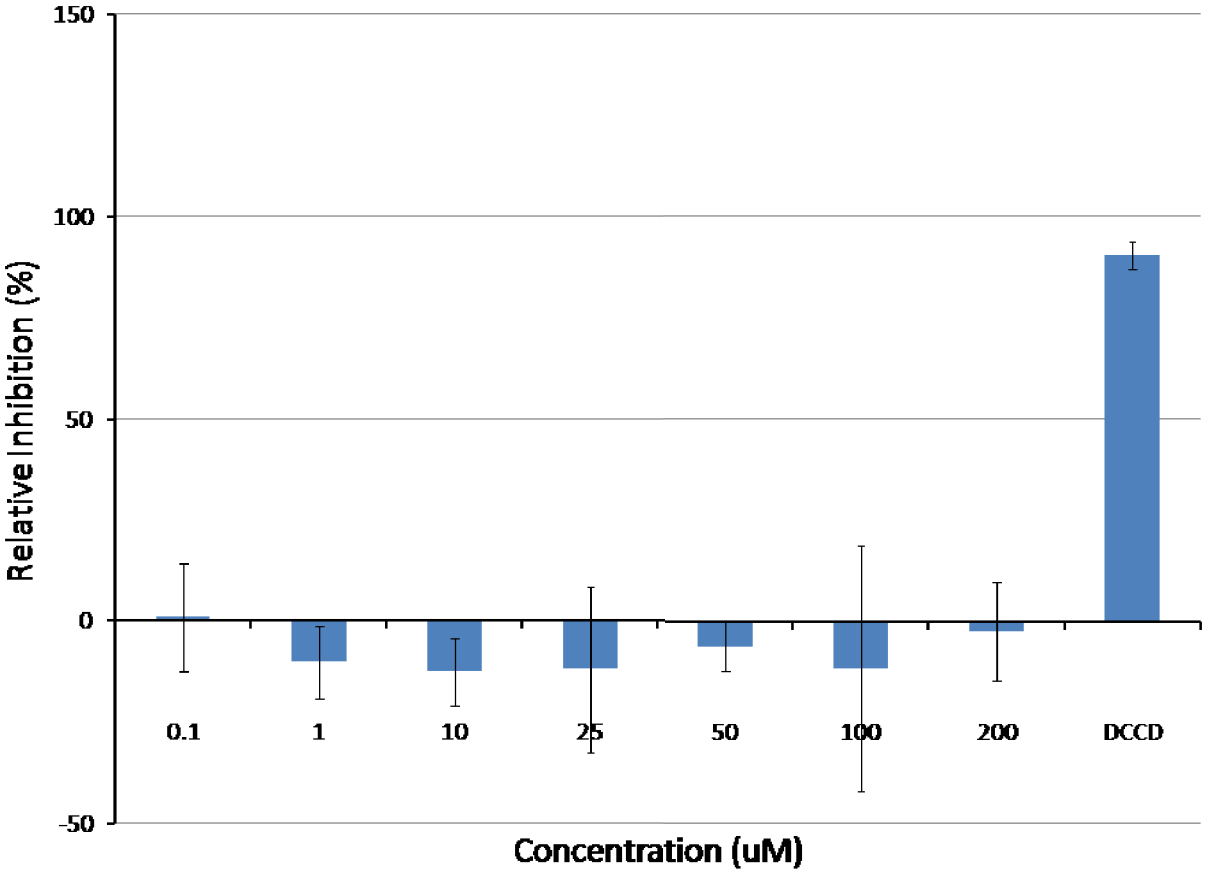

Figure 33. Effect of compound 2 on ATP synthesis in inverted membrane vesicles of *E. coli* RA1 strain using MOPS buffer. The graph represents the mean values of three independent experiments. Inhibition of compound 2 was normalized against DMSO while DCCD was normalized against ethanol. Compound 2 did not display dose-dependent inhibition using MOPS buffer.

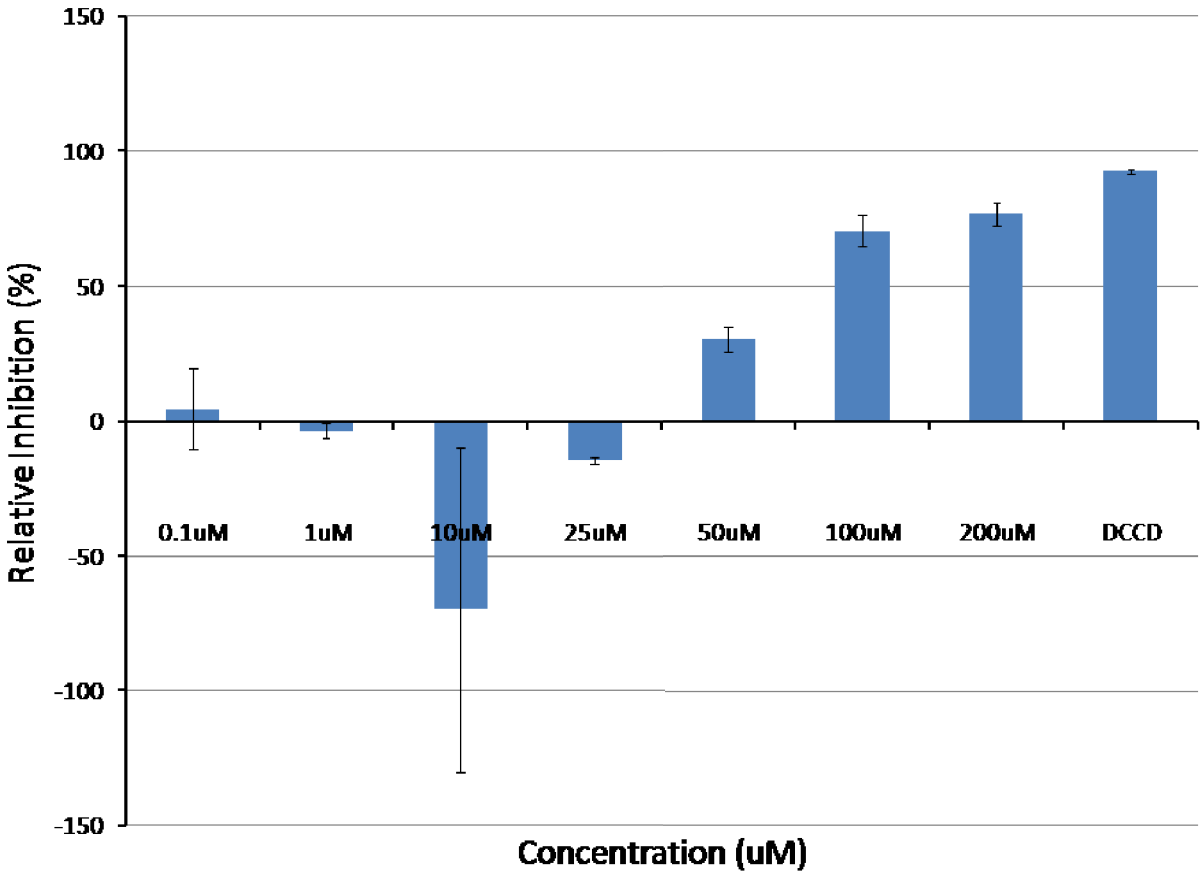

Figure 34. Effect of compound 2 on ATP synthesis in inverted membrane vesicles of *E. coli* RA1 strain using buffer PA4. The graph represents the mean values of three independent experiments. Inhibition of compound 2 was normalized against DMSO while DCCD was normalized against ethanol. Compound 2 displayed some dose-dependent inhibition using buffer PA4.

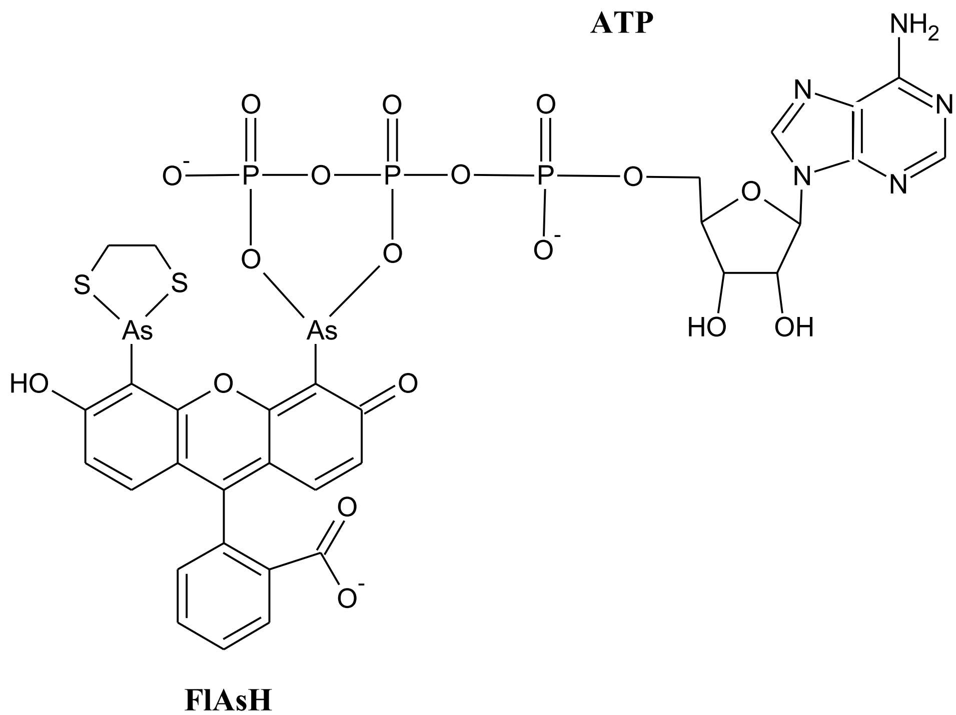

Figure 35. Schematic diagram showing how ATP might bind to FlAsH. The diagram shows that one or both of the arsenic atoms of FlAsH might be able to bind to ATP through the oxygen atoms of its phosphate groups.

9. REFERENCES

Adachi K, Yasuda R, Noji H, Itoh H, Harada Y, Yoshida M, Kinosita K Jr. 2000. Stepping rotation of F1-ATPase visualized through angle-resolved single-fluorophore imaging. Proc Natl Acad Sci U S A 97(13):7243-7.

Adachi K, Oiwa K, Nishizaka T, Furuike S, Noji H, Itoh H, Yoshida M, Kinosita K Jr. 2007. Coupling of rotation and catalysis in F(1)-ATPase revealed by single-molecule imaging and manipulation. Cell 130(2):309-21.

Adams SR and Tsien RY. 2008. Preparation of the membrane-permeant biarsenicals FlAsH-EDT2 and ReAsH-EDT2 for fluorescent labeling of tetracysteine-tagged proteins. Nat Protoc 3(9):1527-34.

Adams SR, Campbell RE, Gross LA, Martin BR, Walkup GK, Yao Y, Llopis J, Tsien RY. 2002. New biarsenical ligands and tetracysteine motifs for protein labeling in vitro and in vivo: Synthesis and biological applications. J Am Chem Soc 124(21):6063-76.

Aggeler R, Ogilvie I, Capaldi RA. 1997. Rotation of a gamma-epsilon subunit domain in the escherichia coli F1F0-ATP synthase complex. the gamma-epsilon subunits are essentially randomly distributed relative to the alpha3beta3delta domain in the intact complex. J Biol Chem 272(31):19621-4.

Amat A, Rigau J, Waynant RW, Ilev IK, Tomas J, Anders JJ. 2005. Modification of the intrinsic fluorescence and the biochemical behavior of ATP after irradiation with visible and near-infrared laser light. J Photochem Photobiol B 81(1):26-32.

Andries K, Verhasselt P, Guillemont J, Gohlmann HW, Neefs JM, Winkler H, Van Gestel J, Timmerman P, Zhu M, Lee E, et al. 2005. A diarylquinoline drug active on the ATP synthase of mycobacterium tuberculosis. Science 307(5707):223-7.

Bald D, Noji H, Yoshida M, Hirono-Hara Y, Hisabori T. 2001. Redox regulation of the rotation of F(1)-ATP synthase. J Biol Chem 276(43):39505-7.

Bienert R, Rombach-Riegraf V, Diez M, Gräber P. 2009. Subunit movements in single membrane-bound H+-ATP synthases from chloroplasts during ATP synthesis. J Biol Chem 284(52):36240-7.

Börsch M, Diez M, Zimmermann B, Reuter R, Gräber P. 2002. Stepwise rotation of the gamma-subunit of EF(0)F(1)-ATP synthase observed by intramolecular single-molecule fluorescence resonance energy transfer. FEBS Lett 527(1-3):147-52.

Boyer PD. 1997. The ATP synthase--a splendid molecular machine. Annu Rev Biochem 66:717-49.

Bradford MM. 1976. A rapid and sensitive method for the quantitation of microgram quantities of protein utilizing the principle of protein-dye binding. Anal Biochem 72:248-54.

Centers for Disease Control and Prevention. Targeted tuberculin testing and treatment of latent tuberculosis infection [Internet]. 2000. Atlanta. Available from: http://www.cdc.gov.library.aucegypt.edu:2048/mmwr/PDF/rr/rr4906.pdf.

Craggs TD. 2009. Green fluorescent protein: Structure, folding and chromophore maturation. Chem Soc Rev 38(10):2865-75.

Didenko VV. 2001. DNA probes using fluorescence resonance energy transfer (FRET): Designs and applications. BioTechniques 31(5):1106,16, 1118, 1120-1.

Diez M, Zimmermann B, Börsch M, Konig M, Schweinberger E, Steigmiller S, Reuter R, Felekyan S, Kudryavtsev V, Seidel CA, et al. 2004. Proton-powered subunit rotation in single membrane-bound F0F1-ATP synthase. Nat Struct Mol Biol 11(2):135-41.

Dounce AL and Rothstein A. 1948. A detailed procedure for the preparation of highly purified adenosine triphosphate. J Biol Chem 174(1):361-70.

Goletti D, Weissman D, Jackson RW, Graham NM, Vlahov D, Klein RS, Munsiff SS, Ortona L, Cauda R, Fauci AS. 1996. Effect of mycobacterium tuberculosis on HIV replication. role of immune activation. J Immunol 157(3):1271-8.

Griffin BA, Adams SR, Tsien RY. 1998. Specific covalent labeling of recombinant protein molecules inside live cells. Science 281(5374):269-72.

Haagsma AC, Abdillahi-Ibrahim R, Wagner MJ, Krab K, Vergauwen K, Guillemont J, Andries K, Lill H, Koul A, Bald D. 2009. Selectivity of TMC207 towards mycobacterial ATP synthase compared with that towards the eukaryotic homologue. Antimicrob Agents Chemother 53(3):1290-2.

Hermanson GT. 1996. Bioconjugate Techniques. San Diego California: Academic Press.

Hisabori T, Kondoh A, Yoshida M. 1999. The gamma subunit in chloroplast F(1)-ATPase can rotate in a unidirectional and counter-clockwise manner. FEBS Lett 463(1-2):35-8.

Hoffmann C, Gaietta G, Bunemann M, Adams SR, Oberdorff-Maass S, Behr B, Vilardaga JP, Tsien RY, Ellisman MH, Lohse MJ. 2005. A FlAsH-based FRET approach to determine G protein-coupled receptor activation in living cells. Nat Methods 2(3):171-6.

Invitrogen. [Internet]. 2010. Carlsbad, California. Available from: http://www.invitrogen.com/site/us/en/home/References/Molecular-Probes-The-Handbook/Thiol-Reactive-Probes/Thiol-Reactive-Probes-Excited-with-Visible-Light.html

Kato-Yamada Y, Noji H, Yasuda R, Kinosita K,Jr, Yoshida M. 1998. Direct observation of the rotation of epsilon subunit in F1-ATPase. J Biol Chem 273(31):19375-7.

Klionsky DJ, Brusilow WS, Simoni RD. 1984. In vivo evidence for the role of the epsilon subunit as an inhibitor of the proton-translocating ATPase of escherichia coli. J Bacteriol 160(3):1055-60.

Ko YH, Hong S, Pedersen PL. 1999. Chemical mechanism of ATP synthase. magnesium plays a pivotal role in formation of the transition state where ATP is synthesized from ADP and inorganic phosphate. J Biol Chem 274(41):28853-6.

Koul A, Vranckx L, Dendouga N, Balemans W, Van den Wyngaert I, Vergauwen K, Gohlmann HW, Willebrords R, Poncelet A, Guillemont J, et al. 2008. Diarylquinolines are bactericidal for dormant mycobacteria as a result of disturbed ATP homeostasis. J Biol Chem 283(37):25273-80.

Koul A, Dendouga N, Vergauwen K, Molenberghs B, Vranckx L, Willebrords R, Ristic Z, Lill H, Dorange I, Guillemont J, et al. 2007. Diarylquinolines target subunit c of mycobacterial ATP synthase. Nat Chem Biol 3(6):323-4.

Lengeler JW, Drews G, Schlegel HG, editors. 1999. Biology of the Prokaryotes. Stuttgart, Germany: Thieme/Blackwell Science. 955 p.

Li C, Numata M, Takeuchi M, Shinkai S. 2005. A sensitive colorimetric and fluorescent probe based on a polythiophene derivative for the detection of ATP. Angew Chem Int Ed Engl 44(39):6371-4.

Mariani F, Goletti D, Ciaramella A, Martino A, Colizzi V, Fraziano M. 2001. Macrophage response to mycobacterium tuberculosis during HIV infection: Relationships between macrophage activation and apoptosis. Curr Mol Med 1(2):209-16.

Mellwig C and Bottcher B. 2003. A unique resting position of the ATP-synthase from chloroplasts. J Biol Chem 278(20):18544-9.

Nishio K, Iwamoto-Kihara A, Tamamoto A, Wada Y, Futai M. 2002. Subunit rotation of ATP synthase embedded in membranes: a or beta subunit rotation relative to the c subunit ring. Proc Natl Acad Sci U S A 99(21):13448-52.

Nishizaka T, Oiwa K, Noji H, Kimura S, Muneyuki E, Yoshida M, Kinosita K,Jr. 2004. Chemomechanical coupling in F1-ATPase revealed by simultaneous observation of nucleotide kinetics and rotation. Nat Struct Mol Biol 11(2):142-8.

Noji H, Yasuda R, Yoshida M, Kinosita K, Jr. 1997. Direct observation of the rotation of F1-ATPase. Nature 386(6622):299-302.

Noji H, Bald D, Yasuda R, Itoh H, Yoshida M, Kinosita K,Jr. 2001. Purine but not pyrimidine nucleotides support rotation of F(1)-ATPase. J Biol Chem 276(27):25480-6.

Noji H, Hasler K, Junge W, Kinosita K, Jr, Yoshida M, Engelbrecht S. 1999. Rotation of escherichia coli F(1)-ATPase. Biochem Biophys Res Commun 260(3):597-9.

Omote H, Sambonmatsu N, Saito K, Sambongi Y, Iwamoto-Kihara A, Yanagida T, Wada Y, Futai M. 1999. The gamma-subunit rotation and torque generation in F1-ATPase from wild-type or uncoupled mutant escherichia coli. Proc Natl Acad Sci U S A 96(14):7780-4.

Pänke O, Gumbiowski K, Junge W, Engelbrecht S. 2000. F-ATPase: Specific observation of the rotating c subunit oligomer of EF(o)EF(1). FEBS Lett 472(1):34-8.

Rao SP, Alonso S, Rand L, Dick T, Pethe K. 2008. The protonmotive force is required for maintaining ATP homeostasis and viability of hypoxic, nonreplicating mycobacterium tuberculosis. Proc Natl Acad Sci U S A 105(33):11945-50.

Reid BG and Flynn GC. 1997. Chromophore formation in green fluorescent protein. Biochemistry 36(22):6786-91.

Ristic Z, Vitali M, Duci A, Goetze C, Kemnitz K, Zuschratter W, Lill H, Bald D. 2009. Two-stimuli manipulation of a biological motor. J Nanobiotechnology 7:3.

Rivers EC and Mancera RL. 2008. New anti-tuberculosis drugs with novel mechanisms of action. Curr Med Chem 15(19):1956-67.

Rosas-Taraco AG, Arce-Mendoza AY, Caballero-Olin G, Salinas-Carmona MC. 2006. Mycobacterium tuberculosis upregulates coreceptors CCR5 and CXCR4 while HIV modulates CD14 favoring concurrent infection. AIDS Res Hum Retroviruses 22(1):45-51.

Sambongi Y, Iko Y, Tanabe M, Omote H, Iwamoto-Kihara A, Ueda I, Yanagida T, Wada Y, Futai M. 1999. Mechanical rotation of the c subunit oligomer in ATP synthase (F0F1): Direct observation. Science 286(5445):1722-4.

Shimabukuro K, Yasuda R, Muneyuki E, Hara KY, Kinosita K, Jr, Yoshida M. 2003. Catalysis and rotation of F1 motor: Cleavage of ATP at the catalytic site occurs in 1 ms before 40 degree substep rotation. Proc Natl Acad Sci U S A 100(25):14731-6.

Suzuki T, Ueno H, Mitome N, Suzuki J, Yoshida M. 2002. F(0) of ATP synthase is a rotary proton channel. obligatory coupling of proton translocation with rotation of c-subunit ring. J Biol Chem 277(15):13281-5.

Taiz L and Zeiger E. 2010. Topic 6.6: Measuring transport in membrane vesicles. Plant Physiology, Fifth Edition Online. Available from:http://5e.plantphys.net/article.php?ch=6&id=53

Tanabe M, Nishio K, Iko Y, Sambongi Y, Iwamoto-Kihara A, Wada Y, Futai M. Rotation of a Complex of the γ Subunit and *c* Ring of *Escherichia coli* ATP Synthase. J Biol Chem 276(18):15269-74.

TB Alliance - Global Alliance for TB Drug Development [Internet]. 2010. New York. Available from: http://www.tballiance.org/why/tb-threat.php

Tsien RY. 1998. The green fluorescent protein. Annu Rev Biochem 67:509-44.

Tsunoda SP, Aggeler R, Yoshida M, Capaldi RA. 2001. Rotation of the c subunit oligomer in fully functional F1Fo ATP synthase. Proc Natl Acad Sci U S A 98(3):898-902.

Tsunoda SP, Aggeler R, Noji H, Kinosita K,Jr, Yoshida M, Capaldi RA. 2000. Observations of rotation within the F(o)F(1)-ATP synthase: Deciding between rotation of the F(o)c subunit ring and artifact. FEBS Lett 470(3):244-8.

Ueno H, Suzuki T, Kinosita K, Jr, Yoshida M. 2005. ATP-driven stepwise rotation of FoF1-ATP synthase. Proc Natl Acad Sci U S A 102(5):1333-8.

von Ballmoos C, Wiedenmann A, Dimroth P. 2009. Essentials for ATP synthesis by F1F0 ATP synthases. Annu Rev Biochem 78:649-72.

Willemse M, Janssen E, de Lange F, Wieringa B, Fransen J. 2007. ATP and FRET--a cautionary note. Nat Biotechnol 25(2):170-2.

World Health Organization [Internet]. 2010a. Geneva. Available from: http://www.who.int/features/qa/08/en/index.html

World Health Organization. Treatment of tuberculosis guidelines [Internet]. 2010b. Geneva. Available from: http://whqlibdoc.who.int/publications/2010/9789241547833_eng.pdf

Yasuda R, Noji H, Kinosita K,Jr, Yoshida M. 1998. F1-ATPase is a highly efficient molecular motor that rotates with discrete 120 degree steps. Cell 93(7):1117-24.

Yasuda R, Noji H, Yoshida M, Kinosita K, Jr, Itoh H. 2001. Resolution of distinct rotational substeps by submillisecond kinetic analysis of F1-ATPase. Nature 410(6831):898-904.

Yoshida M, Muneyuki E, Hisabori T. 2001. ATP synthase--a marvellous rotary engine of the cell. Nat Rev Mol Cell Biol 2(9):669-77.

Zhang J, Campbell RE, Ting AY, Tsien RY. 2002. Creating new fluorescent probes for cell biology. Nat Rev Mol Cell Biol 3(12):906-18.

Zimmermann B, Diez M, Börsch M, Gräber P. 2006. Subunit movements in membrane-integrated EF0F1 during ATP synthesis detected by single-molecule spectroscopy. Biochim Biophys Acta 1757(5-6):311-9.

Zimmermann B, Diez M, Zarrabi N, Gräber P, Börsch M. 2005. Movements of the epsilon-subunit during catalysis and activation in single membrane-bound H(+)-ATP synthase. EMBO J 24(12):2053-63.